Article

Current Biology

The mRNA Decay Factor CAR-1/LSM14 Regulates Axon Regeneration via Mitochondrial Calcium Dynamics

Graphical Abstract

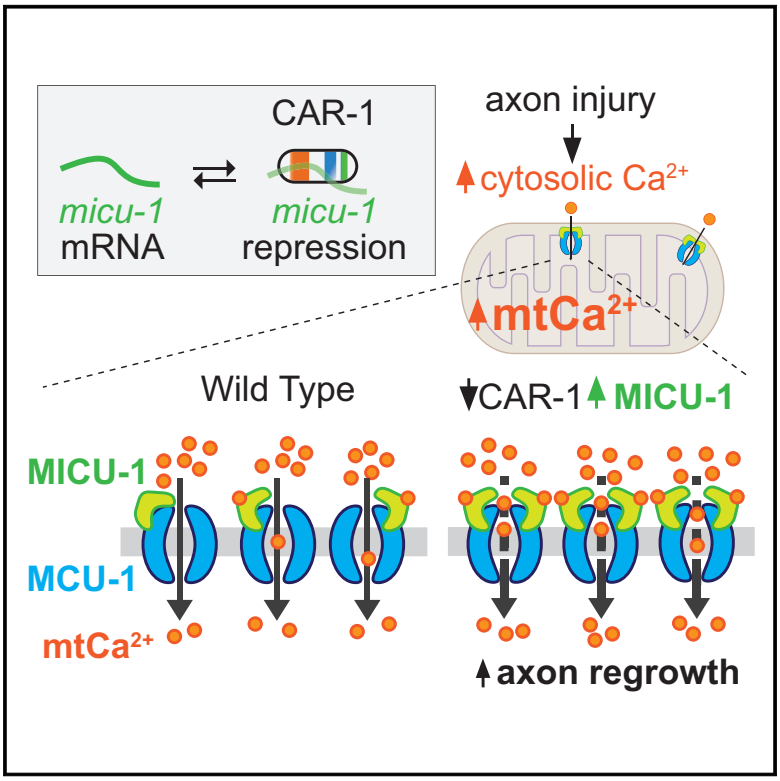

Authors

Ngang Heok Tang, Kyung Won Kim, Suhong Xu, ..., Gene W. Yeo, Yishi Jin, Andrew D. Chisholm

Correspondence

adchisholm@ucsd.edu

In Brief

Tang et al. dissect the roles of mRNA decay factors in *C. elegans* axon regeneration. Loss of function in the LSM14 ortholog CAR-1 results in increased axon regeneration due to elevated expression of MICU-1, a mitochondrial calcium uniporter regulator that is a key target of CAR-1 repression in neurons.

Highlights

- *C. elegans* mRNA decay factors affect axon regeneration and maintenance
- The LSM14 ortholog CAR-1 is a repressor of axon regeneration
- CAR-1 represses expression of the mitochondrial calcium regulator MICU-1
- Axon injury triggers mitochondrial calcium uptake regulated by MICU-1

Tang et al., 2020, Current Biology *30*, 1–12
March 9, 2020
https://doi.org/10.1016/j.cub.2019.12.061

CellPress

Please cite this article in press as: Tang et al., The mRNA Decay Factor CAR-1/LSM14 Regulates Axon Regeneration via Mitochondrial Calcium Dynamics, Current Biology (2019), https://doi.org/10.1016/j.cub.2019.12.061

Current Biology
Article

The mRNA Decay Factor CAR-1/LSM14 Regulates Axon Regeneration via Mitochondrial Calcium Dynamics

Ngang Heok Tang,[1] Kyung Won Kim,[1,3] Suhong Xu,[1,4] Stephen M. Blazie,[1] Brian A. Yee,[2] Gene W. Yeo,[2] Yishi Jin,[1,2] and Andrew D. Chisholm[1,5,*]

[1]Section of Neurobiology, Division of Biological Sciences, University of California, San Diego, La Jolla, CA 92093, USA
[2]Department of Cellular and Molecular Medicine, University of California, San Diego, La Jolla, CA 92093, USA
[3]Present address: Convergence Program of Material Science for Medicine and Pharmaceutics, Department of Life Science, Multidisciplinary Genome Institute, Hallym University, Chuncheon, Republic of Korea
[4]Present address: Center for Stem Cell and Regenerative Medicine, Zhejiang University School of Medicine, Hangzhou 310058, China
[5]Lead Contact
*Correspondence: adchisholm@ucsd.edu
https://doi.org/10.1016/j.cub.2019.12.061

SUMMARY

mRNA decay factors regulate mRNA turnover by recruiting non-translating mRNAs and targeting them for translational repression and mRNA degradation. How mRNA decay pathways regulate cellular function *in vivo* with specificity is poorly understood. Here, we show that *C. elegans* mRNA decay factors, including the translational repressors CAR-1/LSM14 and CGH-1/DDX6, and the decapping enzymes DCAP-1/DCP1, function in neurons to differentially regulate axon development, maintenance, and regrowth following injury. In neuronal cell bodies, CAR-1 fully colocalizes with CGH-1 and partially colocalizes with DCAP-1, suggesting that mRNA decay components form at least two types of cytoplasmic granules. Following axon injury in adult neurons, loss of CAR-1 or CGH-1 results in increased axon regrowth and growth cone formation, whereas loss of DCAP-1 or DCAP-2 results in reduced regrowth. To determine how CAR-1 inhibits regrowth, we analyzed mRNAs bound to pan-neuronally expressed GFP::CAR-1 using a crosslinking and immunoprecipitation-based approach. Among the putative mRNA targets of CAR-1, we characterized the roles of *micu-1*, a regulator of the mitochondrial calcium uniporter MCU-1, in axon injury. We show that loss of *car-1* results increased MICU-1 protein levels, and that enhanced axon regrowth in *car-1* mutants is dependent on *micu-1* and *mcu-1.* Moreover, axon injury induces transient calcium influx into axonal mitochondria, dependent on MCU-1. In *car-1* loss-of-function mutants and in *micu-1* overexpressing animals, the axonal mitochondrial calcium influx is more sustained, which likely underlies enhanced axon regrowth. Our data uncover a novel pathway that controls axon regrowth through axonal mitochondrial calcium uptake.

INTRODUCTION

Mature mRNAs are either actively translated or exist in a translational repressed state that can be targeted for degradation by mRNA decay factors. Extensive biochemical studies show that the recognition of mRNAs by the mRNA decay factor LSM14 and DEAD-box RNA helicase DDX6 leads to translational repression, followed by irreversible removal of the 5′ cap by decapping enzymes DCP1 and DCP2, and mRNA degradation by the exonuclease XRN1 (reviewed in [1]). In multiple cell types, depletion of mRNA decay factors usually leads to accumulation of stabilized mRNAs. However, increasing evidence suggests that mRNA decay factors exhibit a high degree of selectivity in mRNA stability regulation [2]. Therefore, it is crucial to identify the mRNA targets of mRNA decay factors to provide a better understanding of their cellular functions.

Neurons are polarized cells that are primed for a high degree of selective and dynamic regulation of gene expression. mRNA decay factors are widely expressed in neurons of *C. elegans*, *Drosophila*, and mammals [3–6]. For example, *Drosophila* Me31B/DDX6 is enriched in post-synaptic dendrites [5], and its overexpression in sensory neurons reduces higher-order dendrite arborization [3], although it remains unknown whether particular mRNA targets are involved.

C. elegans expresses many conserved mRNA decay factors, whose functions have been mostly characterized in the germline and in early embryos [7–10]. For example, the CAR-1 protein family includes yeast Scd6, *Drosophila* Tral (Trailer hitch), *Xenopus* RAP55, and mammalian LSM14 [11]. The interaction between CAR-1/LSM14 and CGH-1/DDX6 regulates the formation of endoplasmic reticulum and anaphase spindle network; loss of function in *car-1* or *cgh-1* leads to sterility and embryonic lethality due to defects in germline apoptosis and embryonic cytokinesis [7, 8, 10]. Loss of function in *cgh-1* has recently been shown to affect dendrite development in PVD neurons [6]. However, the neuronal mRNA targets of CAR-1 or CGH-1 have not yet been identified.

Here, we show that loss of the translational repressors CAR-1 or CGH-1 results in axon breakage and branching, and increased axon regrowth after injury, whereas loss of mRNA

Please cite this article in press as: Tang et al., The mRNA Decay Factor CAR-1/LSM14 Regulates Axon Regeneration via Mitochondrial Calcium Dynamics, Current Biology (2019), https://doi.org/10.1016/j.cub.2019.12.061

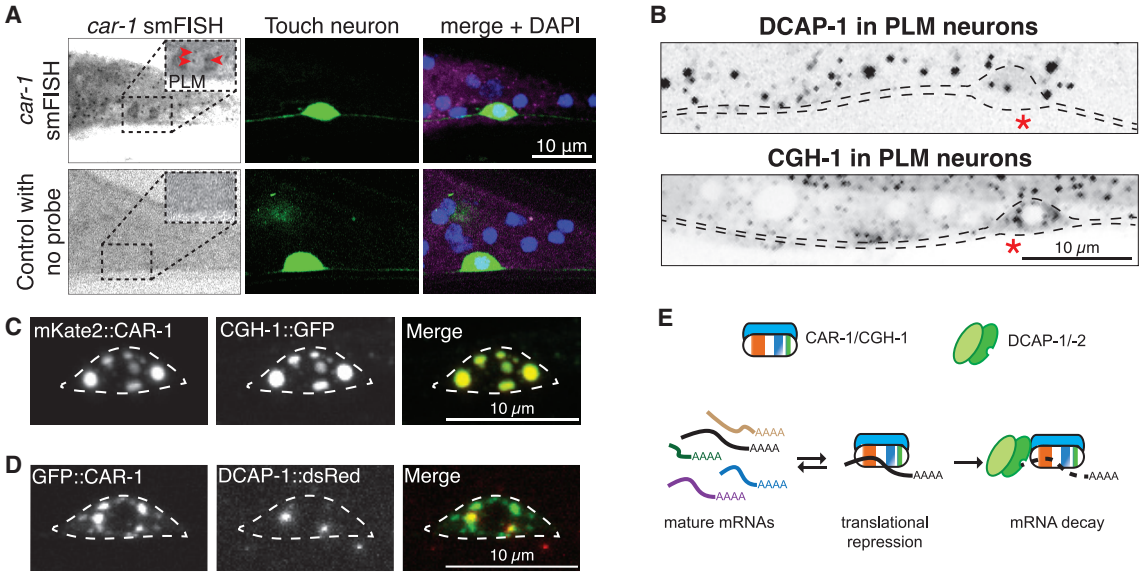

Figure 1. mRNA Decay Components Show Punctate Localization in *C. elegans* Neurons

(A) Single-molecule fluorescence *in situ* hybridization (smFISH) of *car-1* mRNA. Top images showing *car-1* mRNAs form cytoplasmic puncta (red arrowheads) in the PLM neurons. Bottom images show control with no mRNA probe. PLM neurons are labeled with P*mec-7*-GFP (*muIs32*). See also Figures S1 and S2.

(B) *C. elegans* DCAP-1 [P*dcap-1*-DCAP-1::dsRed*(bpIs37)*] or CGH-1 [*Pcgh-1*-CGH-1::GFP*(dhIs1000)*] form puncta in PLM cell bodies. The touch receptor neuron PLM is outlined based on TRN marker in the same image and cell bodies marked by red *. Scale bar, 20 μm.

(C) Confocal images showing co-localization of mKate2::CAR-1 [P*mec-4*-mKate2::CAR-1*(juEx7793)*] and CGH-1::GFP (*dhIs1000*) in the PLM cell body (outlined).

(D) Confocal images show partial co-localization of GFP::CAR-1 [P*mec-4*-GFP::CAR-1*(juSi338)*] and DCAP-1::dsRed (*bpIs37*) in the PLM cell body (outlined). Scale bar, 10 μm.

(E) Model of the relation between the functional complexes containing CAR-1 and CGH-1 and the complexes containing DCAP-1 and DCAP-2. The CAR-1/CGH-1 complex binds to mature mRNAs to repress translation. Translationally repressed mRNAs may be released to allow translation, or decapped and degraded by recruitment of the DCAP-1/DCAP-2 complex.

decapping factors results in aberrant axon development and decreased axon regrowth after injury. We further identified numerous genes including the mitochondrial calcium ($[Ca^{2+}]_{mt}$) regulator *micu-1*, whose mRNAs are bound by CAR-1 in neurons. We present multiple lines of evidence that CAR-1 represses the expression and translation of *micu-1* in neurons. Additionally, we describe a $[Ca^{2+}]_{mt}$ influx induced by axon injury and show that the dynamics of this $[Ca^{2+}]_{mt}$ is regulated by CAR-1 and MICU-1 with dose dependency. Our studies reveal a novel mechanism whereby mRNA decay pathways regulate axonal mitochondrial calcium $[Ca^{2+}]_{mt}$ dynamics.

RESULTS

C. elegans mRNA Decay Factors Are Expressed in Neurons and Localize to Distinct Subcellular Granules

We first asked whether key mRNA decay components were expressed in *C. elegans* neurons. We performed smFISH (single-molecule fluorescence *in situ* hybridization) for endogenous *car-1* mRNAs and observed widespread expression in somatic cells including touch receptor neurons (TRNs) and other neurons besides the germline (Figures 1A and S1). We examined functional transgenes of full-length DCAP-1 or CGH-1 expressed under their respective promoters [12, 13] and observed expression in many neurons including TRNs and motor neurons, localizing to cytoplasmic puncta in neuronal cell bodies (Figures 1B and S2A). To determine protein localization in single neurons, we generated transgenes expressing various mRNA decay factors using the TRN-specific *mec-4* promoter. We found that in TRN cell bodies, CGH-1::GFP fully co-localized with mKate2::CAR-1 puncta (Figure 1C), whereas DCAP-1::dsRed partially co-localized with GFP::CAR-1 (Figure 1D). These results suggest mRNA decay components form at least two types of cytoplasmic granules in *C. elegans* neurons. The partial colocalization of CAR-1 and DCAP-1 further implies that only some CAR-1-bound mRNAs undergo mRNA decapping and decay (Figure 1E).

Assembly of mRNA decay complexes in other organisms involves direct interactions such as binding of DDX6 to LSM14 and of DCP1 to the decapping activator PATL [14, 15]. To address whether punctate localization by *C. elegans* mRNA decay factors depended on similar interactions, we examined genetic null *(0)* mutants. Loss of function in *patr-1*/PATL resulted in fewer DCAP-1 puncta in neurons, whereas loss of function in *cgh-1* resulted in dimmer CAR-1 puncta (Figures S2B and S2C), indicating that PATR-1 and CGH-1 promote recruitment of DCAP-1 and CAR-1, respectively. In contrast, loss of function in decapping enzymes *dcap-1* or *dcap-2* increased the size of CAR-1 puncta (Figure S1C). In *dcap-2(0)* mutants, these enlarged CAR-1 puncta showed nearly complete colocalization with DCAP-1 (Figure S1D), suggesting that the lack of decapping activity may cause accumulation of granules containing CAR-1 and its bound mRNAs.

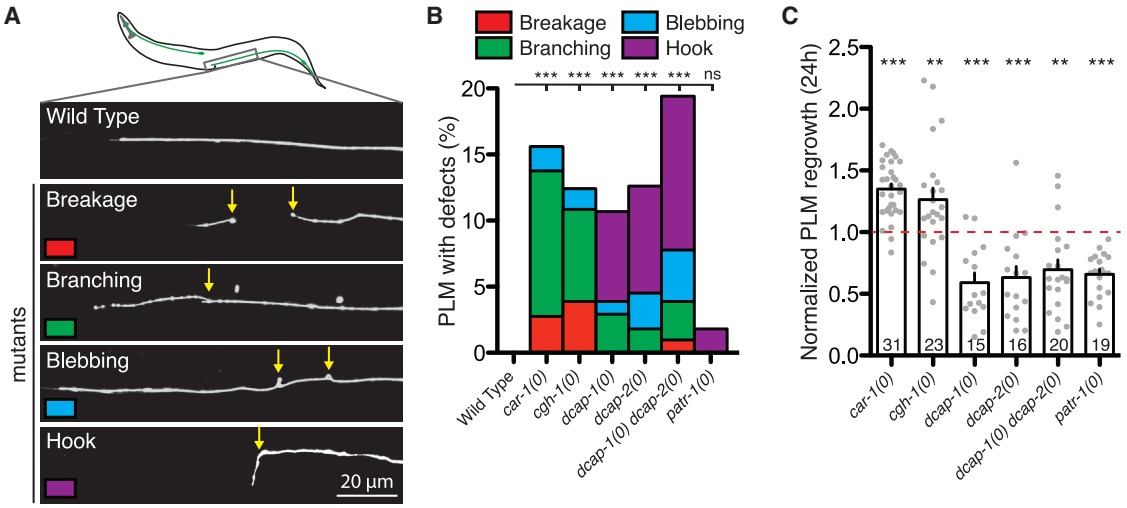

Figure 2. mRNA Decay Components Affect Axon Development, Maintenance, and Regrowth after Injury of PLM Neurons

(A) Top image shows the anterior end of PLM neurons in wild-type animals. Bottom images show abnormal axon morphology observed in mRNA decay mutants (yellow arrows). Scale bar, 20 μm. See also Figure S3.

(B) Quantification of abnormal PLM phenotypes observed in wild-type and mRNA decay mutants. Day 1 adults were observed and quantified. Color correlates to images in (A). $n \geq 100$. Statistics: Fisher's exact test; ***$p < 0.001$; ns, not significant ($p > 0.05$).

(C) Quantification of PLM regrowth length 24 h post-axotomy, normalized to the same-day control animals. Bars indicate mean ± SEM. Statistics: one-way ANOVA with Bonferroni's post test; **$p < 0.01$; ***$p < 0.001$. Sample size is indicated in the bar.

mRNA Decay Components Have Differential Roles in Axon Morphology and Regrowth after Injury

To study the roles of mRNA decay components in neuronal development and maintenance, we focused on the posterior TRN, PLM. In wild-type animals, PLM neurons normally extend a long anterior axon and a short posterior dendrite (Figures 2A and S3A). In *car-1(0)* and *cgh-1(0)* mutant larvae, PLM neurons displayed normal axon morphology (Figure S3B), but in day 1 mutant adults, PLM axons displayed ectopic branching, breakage, and blebbing (Figures 2A, 2B S3A, and S3B), suggesting that*car-1* and *cgh-1* are not essential for PLM axon development, but are necessary for maintaining healthy axon morphology in adults. In contrast, *dcap-1(0)*, *dcap-2(0)*, or *dcap-1(0) dcap-2(0)* mutants at all larval and adult stages displayed low penetrance hook-shaped axon extensions, in addition to ectopic axon branching and blebbing (Figures 2A, 2B, and S3B), suggesting that decapping enzyme activity is important for PLM development.

Adult PLM axons display robust regrowth following femtosecond laser surgery [16]. We next examined how the mRNA decay factors affected axon regrowth. We severed morphologically normal PLM axons in larval (L4) animals lacking specific mRNA decay components and imaged axon regrowth 24 h post-axotomy (hpa). *car-1(0)* and *cgh-1(0)* mutants showed increased regrowth after injury, whereas injured PLM axons in single null mutants for *dcap-1*, *dcap-2*, or *patr-1*, and in *dcap-1(0) dcap-2(0)* double mutants, all showed decreased axon regrowth (Figure 2C). This analysis implies that although these mRNA decay factors can form a protein complex and partly colocalize within the same cell, they exert differential functions in axon development, maintenance, and regrowth. Below, we focus on CAR-1, which is not required for PLM development but is a strong inhibitor of PLM axon regrowth.

CAR-1 Is a Cell-Intrinsic Inhibitor of Axon Regrowth

Three independent *car-1(0)* mutants all exhibited enhanced PLM axon regrowth after injury in the L4 stage, as well as adult-onset axon morphology defects (Figures 3A–3C and S3C). The enhanced regrowth in *car-1(0)* mutants was restored to wild-type levels by single-copy transgenes expressing *car-1* using endogenous or TRN-specific promoters, but not using a muscle-specific promoter (Figure 3B), indicating that CAR-1 regulates axon regrowth cell-autonomously. Axon regrowth involves initial growth cone formation followed by axon extension [17–19]. We observed a higher rate of growth cone formation in *car-1(0)* mutants at multiple time points after axonal injury (Figures 3D and 3E), suggesting that CAR-1 inhibits growth cone formation throughout the process of regrowth. Moreover, overexpression of CAR-1 in TRNs resulted in severe axonal defects in adult animals and strongly impaired axon regrowth and growth cone formation after injury (Figures 3B, 3C, and S3C), indicating that axon maintenance and regrowth are sensitive to CAR-1 levels.

CAR-1 Sm and FDF Domains Are Required for Inhibition of Axon Regrowth

CAR-1 contains three conserved domains (Figure 4A): an N-terminal Sm domain, an FDF (phenylalanine-aspartate-phenylalanine) motif, and a C-terminal RGG (arginine-glycine-glycine) motif [7, 8]. The Sm domain in yeast Scd6 is essential for mRNA translational repression and stimulation of mRNA decay [20], and the FDF motif of *C. elegans* CAR-1 can interact with human DDX6 [14]. We next asked which domain is relevant for CAR-1 cytoplasmic puncta formation and for its function in axon regrowth.

We expressed truncated GFP::CAR-1 in TRNs as single-copy insertion transgenes to ensure consistency in expression level (Figure 4A). We found that the FDF and RGG motifs, but not the Sm domain, contribute to the formation of CAR-1 puncta in

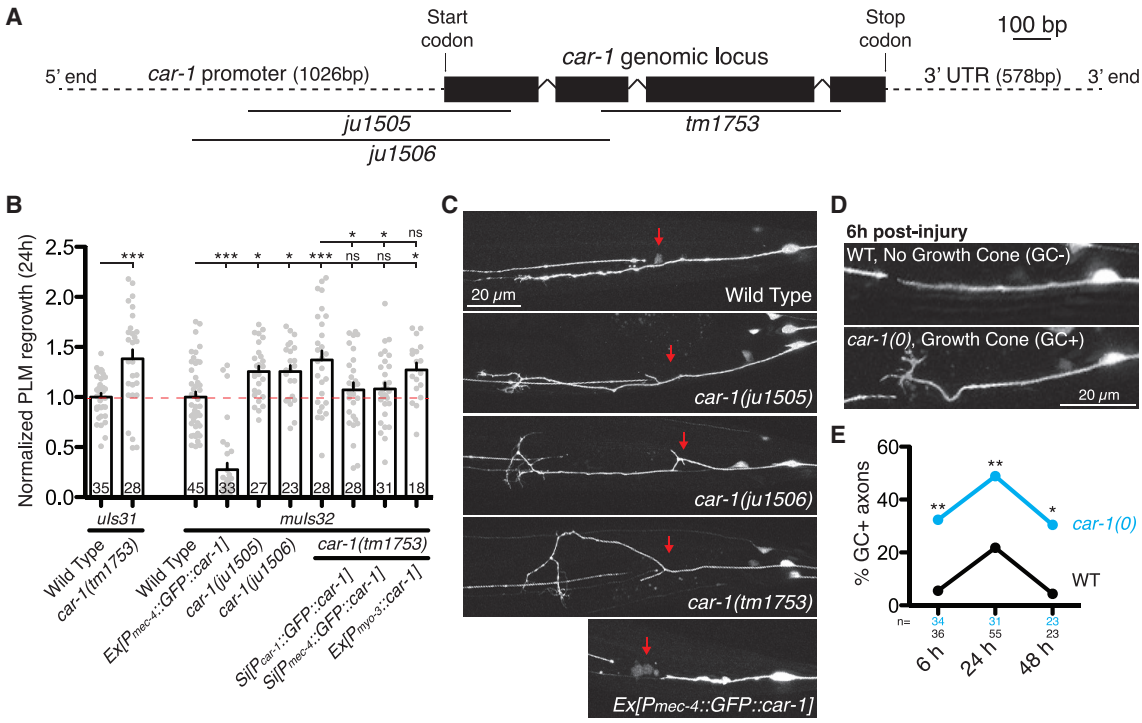

Figure 3. CAR-1 Is a Cell-Intrinsic Inhibitor of Axon Regrowth

(A) Map of *car-1* gene showing deletion mutations. See also Table S2.

(B) PLM axon regrowth length 24 h post-axotomy in genotype indicated. Bars indicate mean ± SEM. Statistics: one-way ANOVA with Bonferroni's post test; *p < 0.05; ***p < 0.001; ns, not significant (p > 0.05). Sample size is indicated in the bar.

(C) Representative images of axon regrowth 24 h post-axotomy in wild-type, *car-1(0)* mutants, and P*mec-4*-GFP::CAR-1(*juEx7280*). Anterior is to the left. Red arrows indicate site of axotomy.

(D) Representative images of re-growing axons 6 h post-axotomy in genotype indicated. PLM in *car-1(0)* mutants has a more persistent regenerative growth cone. Scale bar, 20 μm.

(E) Quantitation of percentage of growth cones at 6, 24, and 48 h post-axotomy. Statistics: Fisher's exact test; *p < 0.05; **p < 0.01.

PLM cell bodies (Figure 4A), consistent with observations in *C. elegans* embryos [7]. To address the function of CAR-1 mutant proteins, we performed axon injury in *car-1(0)* animals expressing each transgene. Expression of CAR-1(FL) or CAR-1(Sm+FDF), but not CAR-1(Sm), CAR-1(ΔSm), CAR-1(RGG), nor CAR-1(ΔFDF+RGG), in *car-1(0)* mutants restored axon regrowth and growth cone formation to wild-type levels (Figures 4B and 4C). These data indicate that the Sm domain and FDF motif of CAR-1, hence its role in RNA translational repression, are critical for CAR-1 function in neurons.

CAR-1 Regulates Its mRNA Expression in PLM Neurons

To identify neuronal targets of CAR-1, we constructed transgenic strains overexpressing GFP::CAR-1(FL) (*juIs526*) or GFP::CAR-1(ΔSm) (*juIs549*) in all neurons using the pan-neuronal *rgef-1* promoter. In axon injury assay, we found that overexpression of GFP::CAR-1(FL), but not GFP::CAR-1(ΔSm), inhibited PLM axon regrowth (Figure 5A), confirming the importance of the Sm domain in CAR-1 function. We then performed single-end enhanced crosslinking and immunoprecipitation (seCLIP) to isolate mRNA targets of CAR-1 using these transgenic animals (see STAR Methods for details) [21, 22]. We reasoned that mRNAs repressed by CAR-1 should be more stably bound to non-functional GFP::CAR-1(ΔSm) than to GFP::CAR-1(FL). We analyzed seCLIP data to identify peaks specifically enriched in GFP::CAR-1(ΔSm) samples (STAR Methods) and selected about 30 or so potential targets (Table S1). Among them, we found that *car-1* itself was specifically enriched in GFP::CAR-1(ΔSm) co-immunoprecipitates (Figure 5B), suggesting CAR-1 might repress its own expression. To test this, we performed smFISH for *car-1* in animals expressing P*mec-4*::GFP::CAR-1 and found that *car-1* mRNA puncta partly colocalized with GFP::CAR-1 cytoplasmic puncta in wild-type and *dcap-2(0)* animals (Figure 5C). Since *cgh-1(0)* mutants display dimmer GFP::CAR-1 puncta (Figure S1C), we visualized *car-1* mRNAs in *cgh-1(0)* mutants and observed that *cgh-1(0)* mutants displayed more *car-1* mRNA puncta (Figures 5D and 5E), suggesting that *car-1* mRNA levels are normally limited by CAR-1/CGH-1 activity.

CAR-1 Binds *micu-1* Transcripts and Represses MICU-1::GFP Protein Levels in PLM Neurons

We identified 29 genes whose mRNAs showed enriched peaks in GFP::CAR-1(ΔSm) seCLIP analysis, including several calcium-related genes: *clp-1*, *kcnl-1*, *micu-1*, and *unc-13* (Table S1). Several genes were previously analyzed for their roles in PLM axon regrowth [18, 23]. Given recent evidence for the function of mitochondria in axon regrowth [24–26], here we chose to

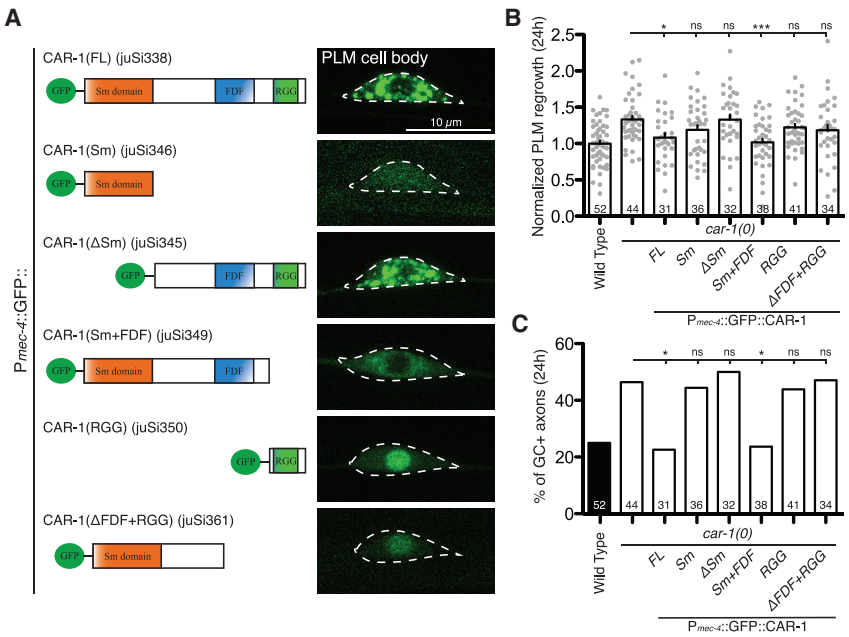

Figure 4. The Sm Domain and FDF Motif Are Required for CAR-1 Function in Axon Regrowth

(A) Cytoplasmic puncta formation by truncated CAR-1 proteins. Left: schematic of truncated CAR-1 fragments fused to GFP in the N terminus. Right: confocal images showing localization of GFP::CAR-1 constructs.

(B) Increased PLM axon regrowth length in *car-1(0)* is restored to wild-type levels by P*mec-4*-GFP::CAR-1-FL*(juSi338)* and P*mec-4*-GFP::CAR-1ΔRGG *(juSi349)*. Bars indicate mean ± SEM. Statistics: one-way ANOVA with Bonferroni's post test; *p < 0.05; ***p < 0.001; ns, not significant.

(C) Increased growth cone formation in *car-1(0)* is restored to wild-type level by P*mec-4*-GFP::CAR-1-FL*(juSi338)* and P*mec-4*-GFP::CAR-1ΔRGG *(juSi349)*. Statistics: Fisher's exact test; *p < 0.05; ns, not significant. Sample size is indicated in the bar.

focus on *micu-1*, which encodes a mitochondrial calcium uptake regulator of the MICU1 family (Figure S4A). Careful inspection of the seCLIP peak profiles revealed that GFP::CAR-1(ΔSm) samples were specifically enriched on *micu-1* (Figure 5B). To further verify this finding, we performed smFISH of *micu-1* mRNA. In wild type PLM neurons, *micu-1* mRNA puncta partly colocalized with GFP::CAR-1 (Figure 6A), similar to *car-1* mRNA. In *car-1(0)* mutants, we observed increased numbers of *micu-1* mRNA puncta in PLM cell bodies (Figures 6B and 6C). The increased *micu-1* mRNA puncta observed in *car-1(0)* mutant TRNs was suppressed by expressing CAR-1(FL) or CAR-1(Sm+FDF), but not CAR-1(ΔSm) (Figure 6C), suggesting that CAR-1(Sm) domain mediates translational repression. *micu-1* mRNA puncta did not colocalize with GFP::DCAP-1 (Figure S5A), suggesting that DCAP-1 does not regulate expression of *micu-1* mRNA directly.

Next, we characterized endogenous MICU-1 expression by inserting GFP into the carboxy-terminus of the endogenous *micu-1* gene (see STAR Methods). MICU-1::GFP was detected at low levels in germ cells, epidermis, and some muscles (Figure S4B). MICU-1::GFP was detected at low levels in PLM neuron soma, colocalizing with a mitochondrial marker, but was below the limit of detection in axons (Figure 6D). As *micu-1* transcript levels were increased in *car-1(0)* mutants, we examined whether MICU-1::GFP signals were different in *car-1(0)* mutant compared to wild type. We observed a consistent 1.2-fold increase of MICU-1::GFP intensity in PLM cell bodies in *car-1(0)* mutant compared to wild type (Figures 6E and 6F). Collectively, these observations indicate that CAR-1 binds *micu-1* mRNA and represses its translation in PLM neurons.

CAR-1-Mediated Inhibition of Axon Regrowth Is Dependent on the Mitochondrial Calcium Import Factors MCU-1 and MICU-1

MICU1 is an EF-hand protein that forms a complex with the MCU1 uniporter to regulate $[Ca^{2+}]_{mt}$ uptake [27–31]. We therefore hypothesize that axonal mitochondrial calcium uptake might influence regrowth dynamics. To test this, we first asked whether *micu-1*, or the uniporter *mcu-1*, affected PLM axon regrowth. We analyzed axon regrowth in double mutants between *car-1(0)* and *mcu-1(0)* or *micu-1(0)*. Loss of *mcu-1* or *micu-1* fully suppressed increased axon regrowth observed in *car-1(0)* mutants (Figure 7A). However, loss of *mcu-1* or *micu-1* did not suppress the increased growth cone formation observed in *car-1(0)* mutants, indicating that CAR-1 acts via other targets to regulate axon extension and growth cone formation. *micu-1(0)* also suppressed the adult-onset axon maintenance defects of *car-1(0)* mutants (Figure S5B), suggesting that MICU-1 is acting downstream of CAR-1 in axon maintenance. Loss of *mcu-1* or *micu-1* did not rescue axon regrowth and axon morphology defects of *dcap-1(0)* mutants (Figures S5C and S5D), implying that *micu-1* is a specific target of CAR-1 but not of DCAP-1.

Axon Injury Triggers Mitochondrial Calcium Uptake Dependent on MCU-1 and Regulated by MICU-1

We next addressed whether axon injury might affect $[Ca^{2+}]_{mt}$ flux. We targeted the Ca^{2+} sensor GCaMP5 to the mitochondrial matrix (mtGCaMP) in TRNs. *micu-1(0)*, *mcu-1(0)*, and *car-1(0)* mutants displayed normal axonal mitochondrial distribution and baseline mtGCaMP levels (Figures S6A and S6B). We confirmed that injury causes a cytosolic Ca^{2+} ($[Ca^{2+}]_c$) transient (Figure 7B) [32], with no significant difference between wild-type, *car-1(0)*, *mcu-1(0)*, and *micu-1(0)* mutants (data not shown).

In wild-type PLM axons, injury triggered a rapid increase in mtGCaMP fluorescence, consistent with axonal $[Ca^{2+}]_{mt}$ uptake (Figures 7B and 7C). We measured the relative change in mtGCaMP fluorescence (ΔF/F0) and found that the increased mtGCaMP fluorescence peaked within seconds of injury followed by decay to baseline levels after 5 min (Figures 7B–7D). Loss of function in *mcu-1* abolished the axotomy-triggered mtGCaMP transient (Figure 7B). In contrast, *micu-1(0)* PLM axons showed a higher peak mtGCaMP fluorescence immediately after injury but decayed faster, and by 5 min after injury,

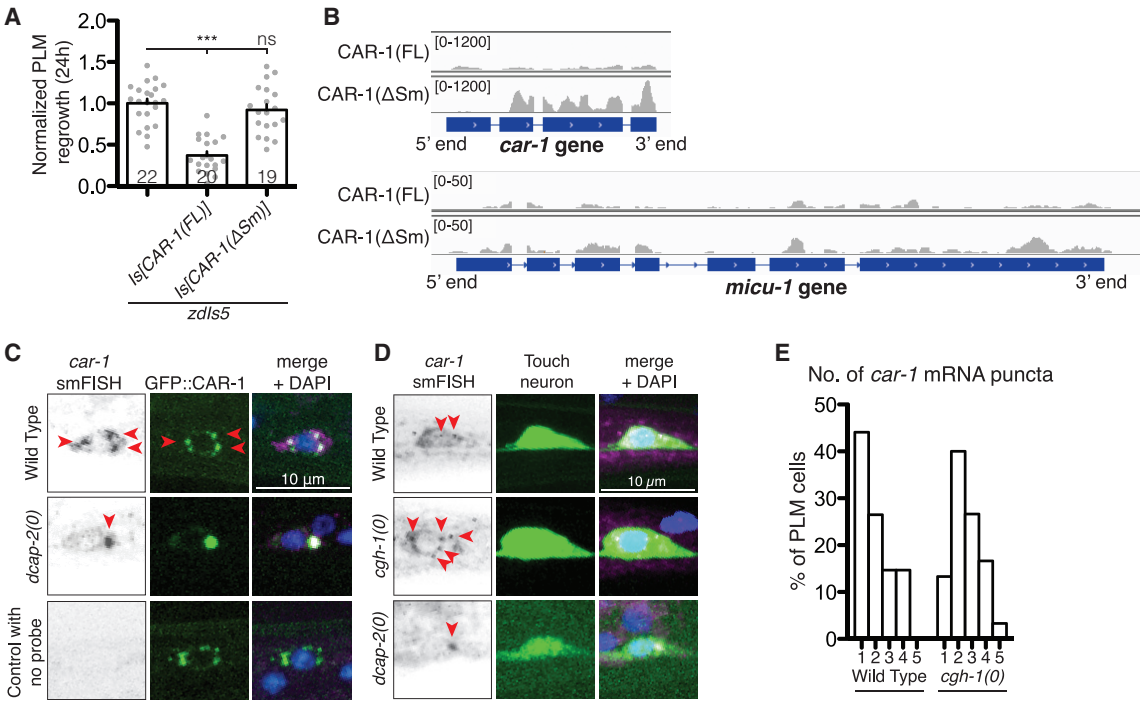

Figure 5. CAR-1 Regulates Its mRNA Expression in PLM Neurons

(A) PLM axon regrowth length 24 h post-axotomy in transgenic animals overexpressing CAR-1(FL)*(juIs526)* or CAR-1(ΔSm)*(juIs549)* driven by the pan-neuronal promoter P*rgef-1*. Bars indicate mean ± SEM. Statistics: one-way ANOVA with Bonferroni's post test; ***$p < 0.001$; ns, not significant.

(B) seCLIP-read density track on *car-1* and *micu-1* gene for CAR-1(FL) and CAR-1(ΔSm) samples. Distinct peaks were enriched in the CAR-1(ΔSm) sample. See also Table S1.

(C) smFISH shows colocalization of *car-1* mRNA (red arrowheads) with GFP::CAR-1 protein in the PLM cell body. Cytoplasmic puncta of *car-1* mRNAs co-localize with CAR-1 protein in wild type and enlarge in *dcap-2(0)* backgrounds.

(D) smFISH of *car-1* mRNAs (red arrowheads). The number of *car-1* mRNA puncta increases in *cgh-1(0)*, whereas in *dcap-2(0)* mutants, *car-1* mRNAs accumulate in a large punctum.

(E) Quantification of *car-1* mRNA puncta in PLM cell bodies of wild-type and *cgh-1(0)* mutant, expressed as percentage of PLM cells with one, two, three, etc. puncta. Representative images shown in (D). $n \geq 30$ for each strain.

had mtGCaMP levels similar to wild-type animals (Figure 7B). The increase in mtGCaMP fluorescence observed in wild-type and *micu-1(0)* axons after injury was dependent on MCU-1, because *mcu-1(0) micu-1(0)* double mutants did not display any transient mtGCaMP increase following axonal injury, resembling *mcu-1* single mutants (Figure 7B). Our results show that MCU-1 is essential for the transient $[Ca^{2+}]_{mt}$ uptake after axon injury, whereas MICU-1 appears to inhibit initial Ca^{2+} overload, consistent with the gatekeeping function of mammalian MICUs [30, 33, 34].

car-1(0) Mutants Display More Sustained Axonal $[Ca^{2+}]_{mt}$ Uptake

We further addressed whether the axotomy-triggered $[Ca^{2+}]_{mt}$ influx was regulated by CAR-1 by examining $[Ca^{2+}]_{mt}$ uptake in *car-1(0)* animals. The mtGCaMP transients triggered immediately (2.4 s after axotomy) by injury in *car-1(0)* were similar to those in wild-type axons (Figures 7B and 7C). However, *car-1(0)* mutants displayed a more sustained elevation in $[Ca^{2+}]_{mt}$ levels compared to wild type; this elevation was completely dependent on MCU-1 (Figures 7B–7D). As expression of MICU-1 was elevated in *car-1(0)* mutants (Figure 6), we next tested whether loss of *micu-1* was able to restore wild-type $[Ca^{2+}]_{mt}$ levels in *car-1(0)* mutants. We observed wild-type $[Ca^{2+}]_{mt}$ levels in *car-1(0)* and *micu-1(0)* double mutants (Figure 7B). Further, slight elevation of *micu-1* levels in the TRNs resulted in increased axon regrowth and sustained axonal $[Ca^{2+}]_{mt}$ uptake after injury (Figures S7A–S7C). Axon regrowth was impaired when *micu-1* was overexpressed to a high level (Figure S7A), suggesting axon regrowth is sensitive to the level of MICU-1. Overall, our results suggest that mild elevation of MICU-1 expression is responsible for the more sustained $[Ca^{2+}]_{mt}$ uptake and increased axon regrowth of *car-1(0)* mutants upon axon injury.

DISCUSSION

In this study, we find that CAR-1 and other mRNA decay factors play multiple roles in *C. elegans* axon development, axon maintenance, and axon regrowth. We further dissected the mechanism by which CAR-1 inhibits axon regrowth after injury. We presented multiple lines of evidence that the mitochondrial calcium regulator MICU-1 is a major CAR-1 target in axon regrowth. We also show that the regulation of MICU-1 by CAR-1

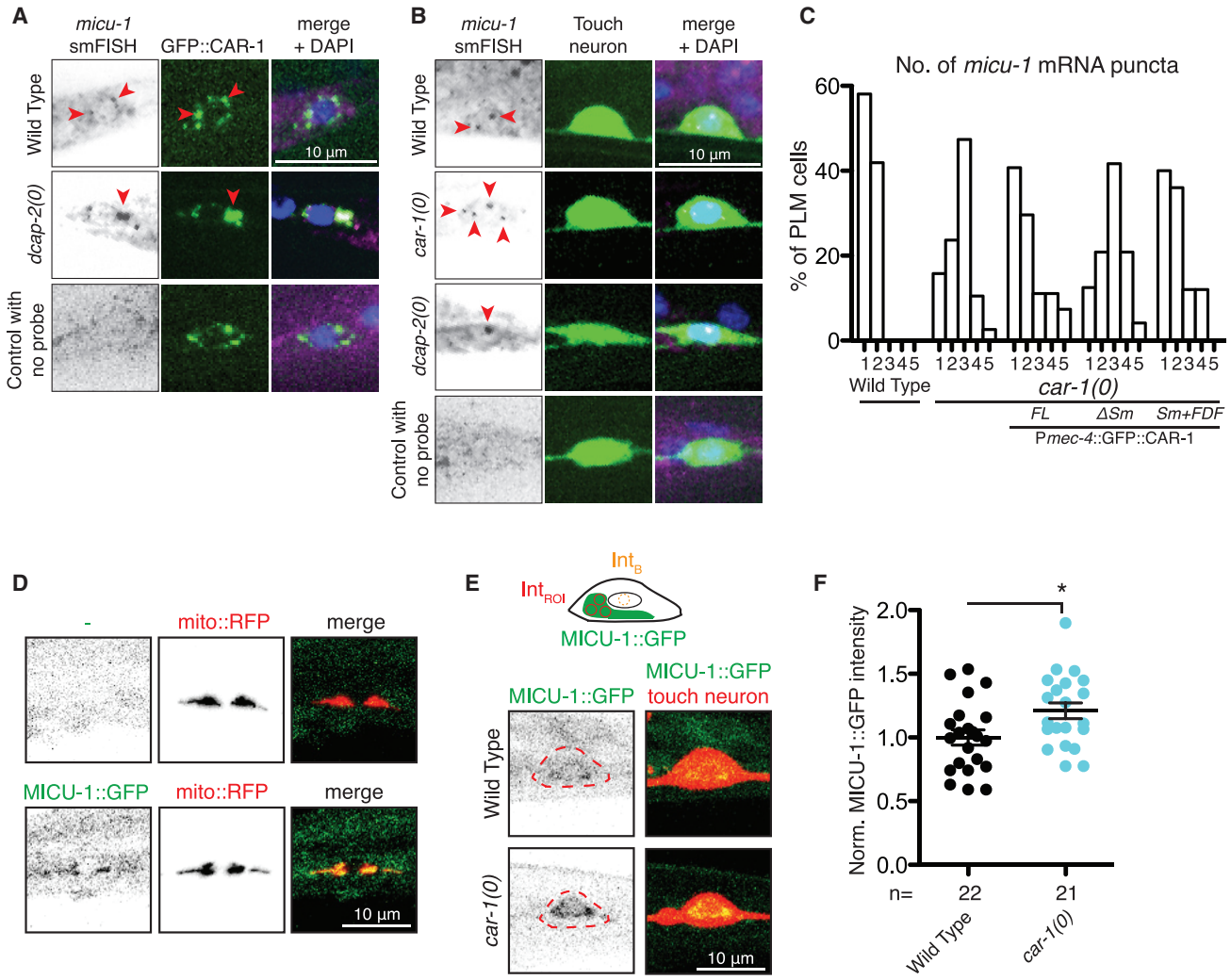

Figure 6. CAR-1 Regulates *micu-1* Transcript Levels and Represses MICU-1::GFP Protein Levels

(A) smFISH shows colocalization of *micu-1* mRNA with GFP::CAR-1 in the PLM cell body. Cytoplasmic puncta of *micu-1* mRNAs (red arrowheads) co-localize with CAR-1 protein puncta in the PLM cell body in wild-type and *dcap-2(0)* mutant. See also Figures S4 and S5.

(B) smFISH of *micu-1* mRNAs (red arrowheads) shows *micu-1* mRNAs form cytoplasmic puncta in PLM neurons, labeled with P*mec-7*-GFP *(muls32)*. More *micu-1* mRNA puncta in *car-1(0)* mutants and increased accumulation in *dcap-2(0)* mutants were observed.

(C) Quantification of *micu-1* mRNA puncta in PLM cell bodies of wild-type and *car-1(0)* mutants. Representative images shown in (E). n ≥ 24 for each strain.

(D) Top shows confocal images of mito::RFP [P*mec-7*-tagRFP-mito(*jsIs1073*)] in the absence of MICU-1::GFP(*ju1783*). Bottom shows confocal images showing colocalization of MICU-1::GFP(*ju1783*) with mito::RFP in the PLM cell bodies.

(E) Top is an illustration of the region of interest (Int_{ROI}) and background (Int_B). Bottom images show MICU-1::GFP(*ju1783*) in PLM cell bodies (outlined), with increased expression in *car-1(0)*. Scale bar, 10 µm.

(F) MICU-1::GFP intensities in wild type and *car-1(0)* animals, normalized to wild-type control. Statistics: unpaired Student's t test; *p = 0.0194.

is important for fine-tuning injury-induced $[Ca^{2+}]_{mt}$ transients. Our data reveal a previously unknown molecular pathway linking mRNA decay and axonal $[Ca^{2+}]_{mt}$ dynamics.

Our analyses on *C. elegans* mRNA decay factors are consistent with an emerging notion that these factors have distinct *in vivo* functions. Focusing on the PLM neurons, we show that mRNA decay factors localize to at least two main subcellular granules, as the decapping enzymes are present in a subset of granules containing translational repressors. These observations are consistent with reports that in *Drosophila* neurons, decapping enzymes partly colocalize with the translational repressor Me31B/DDX6 [5]. Our data further show that mRNA decapping factors DCAP-1 and DCAP-2 are required for PLM developmental axon guidance and regrowth, whereas translational repressors CAR-1 and CGH-1 are not essential for PLM axon development but inhibit PLM axon regrowth and maintain adult axon integrity. We have found that MICU-1, a member of a highly conserved family of $[Ca^{2+}]_{mt}$ regulators, is a major functionally relevant target of neuronal CAR-1. *micu-1* transcripts are present in CAR-1-positive, DCAP-1-negative granules, suggesting different mRNA decay factors regulate expression of distinct mRNA targets. Our observation that in

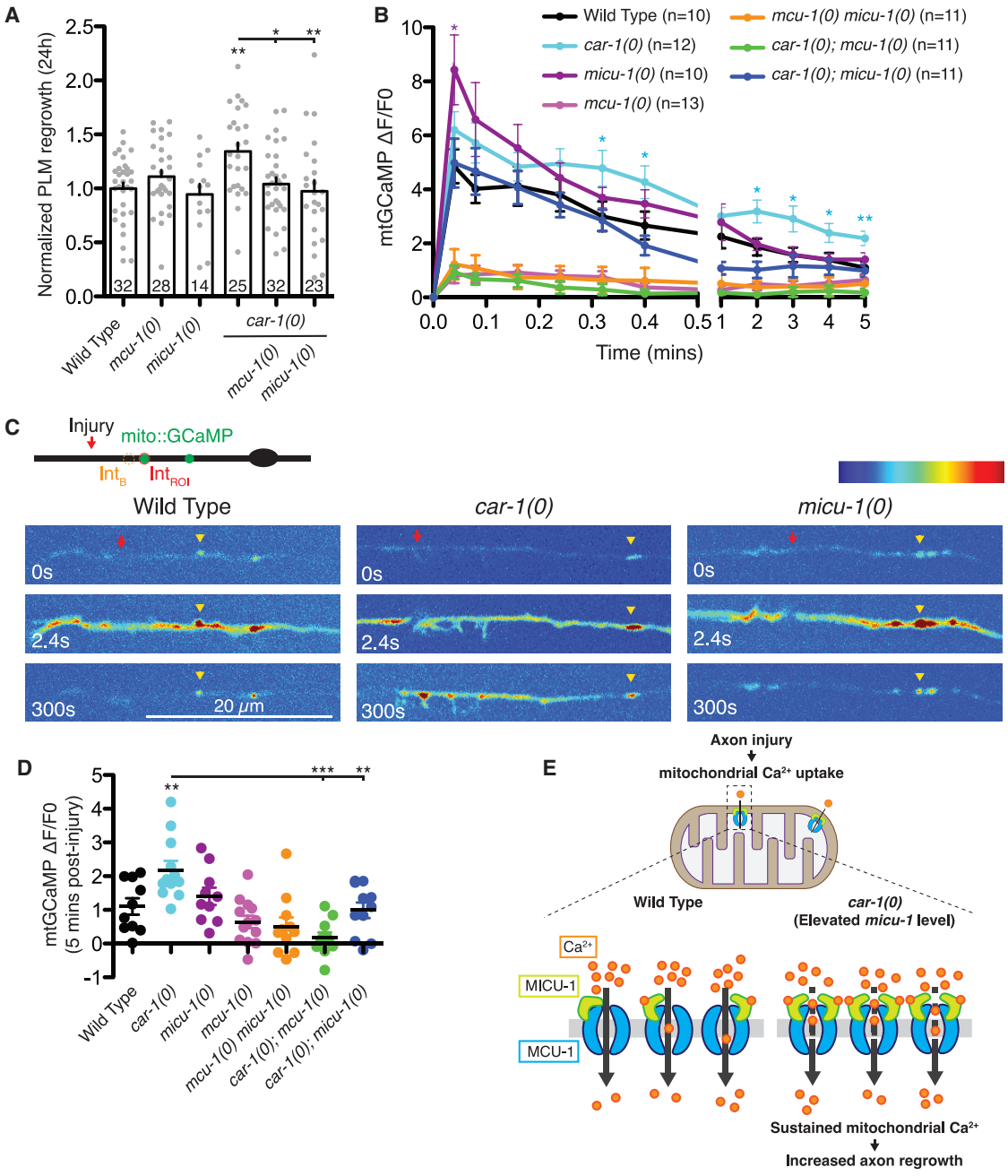

Figure 7. CAR-1 Represses Axonal Mitochondrial Calcium Uptake after Axon Injury

(A) PLM regrowth length 24 h post-axotomy. Statistics: one-way ANOVA with Bonferroni's post test; *p < 0.05; **p < 0.01. Sample size is indicated in the bar. See also Figures S5, S6, and S7.

(B) mtGCaMP fluorescence intensity (ΔF/F0) over 5 min post-axotomy. Statistics: unpaired t test against wild type; *p < 0.05; **p < 0.01.

(C) Top is an illustration of the region of interest (Int_{ROI}) and background (Int_B). Bottom images show mitochondrial calcium imaging trace in wild type, *car-1(0)*, and *micu-1(0)* mutant axons post-axotomy. Animals expressing the mtGCaMP sensor [P*mec-4*-mito-GCaMP5(*juIs550*)] were severed using femtosecond laser and imaged immediately. Red arrows show the cut site. Yellow arrowheads mark mitochondria in PLM neurons. Some mtGCaMP signal is in the neuronal cytoplasm, likely reflecting incomplete targeting of mtGCaMP due to the high copy number of *juIs550*. Scale bar, 20 μm.

(D) mtGCaMP fluorescence intensity (ΔF/F0) at 5 min post-axotomy in genotypes indicated. Each dot represents the 5-min mtGCaMP 5 min post-injury in a single animal. Statistics: unpaired t test; **p < 0.01; ***p < 0.001.

(E) Model for regulation of axon regrowth by CAR-1 and $[Ca^{2+}]_{mt}$ uptake. Axon injury induces transient mitochondrial Ca^{2+} uptake, dependent on MCU-1. Loss of CAR-1 results in elevated *micu-1* mRNA expression, leading to more sustained mitochondrial Ca^{2+} uptake after injury, correlating with increased axon regrowth.

the absence of DCAP-1 or DCAP-2, the mRNA targets of CAR-1 accumulate in larger CAR-1 granules, suggests that increased binding of CAR-1 to its mRNA targets likely leads to translational repression, potentially accounting for the axonal developmental defects and decreased axon regrowth in decapping enzyme mutants.

We find that at least two domains of LSM14 family proteins are important for translational repression. The Sm domain is essential for binding to 4E-T, and the FDF domain binds to DDX6/CGH-1 and serves as a platform for other mRNA decay factors [14, 35]. We find that truncated CAR-1(Sm+FDF) protein can suppress the increased *micu-1* transcript level of *car-1(0)* mutants, despite not forming distinct puncta in neurons. Our findings are consistent with prior studies showing the RGG motif is dispensable for translational repression [36, 37]. Moreover, translational repression has been observed in the absence of visible cytoplasmic puncta formation [38, 39]. Taken together, our results suggest that CAR-1 may bind to and repress translation of mRNA targets even in the absence of visible puncta.

Through characterizing *in vivo* mRNA targets of CAR-1 in neurons, we have uncovered a previously unknown pathway involving mitochondria calcium regulation in axon injury. The functions of mitochondrial calcium uniporter MCU complex critically depend on its regulatory subunits, including the MICU proteins and cytoplasmic calcium (reviewed in [40, 41]), and are important for human health. Mutations in human MICU genes have been linked to neurological disorders [42–44], and MCU itself is implicated in excitotoxic neuronal cell death [45]. $[Ca^{2+}]_{mt}$ dynamics affect multiple aspects of cellular metabolism, including oxidative phosphorylation, Ca^{2+} buffering, and reactive oxygen species production, so abnormal $[Ca^{2+}]_{mt}$ dynamics could affect neuronal development and function in several ways [46]. Emerging evidence links elevated $[Ca^{2+}]_{mt}$ uptake to axonal degeneration in vertebrates [47, 48] and in *C. elegans* [49]. Moreover, increased Ca^{2+} levels in traumatic brain injury can be ameliorated by the inhibition of MCU1 [50], suggesting potential therapeutic benefits of mitochondrial Ca^{2+} regulation in brain injury. Loss of function in *Drosophila* MCU or MICU causes aberrant axon morphology and impairs memory formation [51]. Interestingly, expression levels of MCU and MICU are dependent on neuronal cell type and Ca^{2+} signaling [52]. Our results reveal that neuronal MICU-1 levels are fine-tuned by the mRNA decay machinery, adding another level of regulation to neuronal $[Ca^{2+}]_{mt}$ dynamics.

Axon injury triggers a transient elevation in $[Ca^{2+}]_c$ [17, 32, 53]. In *C. elegans* neurons, increased $[Ca^{2+}]_c$ could contribute to the activation of the conserved kinase DLK-1, thereby promoting axon regrowth [54, 55]. Here, we reveal that axon injury also triggers axonal $[Ca^{2+}]_{mt}$ uptake in *C. elegans*, reminiscent of observations in vertebrate neurons [56]. We find that this $[Ca^{2+}]_{mt}$ uptake is completely dependent on MCU-1 and is regulated in complex ways by MICU-1. In cultured mammalian cells, MICU1 localizes to mitochondria [31, 57–59] and inhibits MCU function at low $[Ca^{2+}]_c$ levels (known as "gatekeeping"), but at higher $[Ca^{2+}]_c$ levels, Ca^{2+} binds to MICU1 to stimulate MCU1 opening [33, 34, 59]. MICU1 therefore can inhibit or promote MCU function depending on the $[Ca^{2+}]_c$ level. Supporting this model, our data show that loss of function in *micu-1* and *mcu-1* have opposing effects on the amplitude of the initial $[Ca^{2+}]_{mt}$ transient after axotomy. However, the enhanced axon regrowth of *car-1(0)* mutants is suppressed to a similar degree by loss of function in *mcu-1* or *micu-1*. Our data suggest that the MCU-1-stimulating role of MICU-1 at lower $[Ca^{2+}]_c$ is most relevant to the long-term outcome in axon regrowth.

MCU function is sensitive to the stoichiometry of MICU and other regulatory subunits. For example, liver mitochondria have a higher MICU1:MCU1 ratio than heart or muscle mitochondria and display increased cooperativity of $[Ca^{2+}]_{mt}$ uptake [60]. We propose that in PLM neurons, CAR-1 tightly regulates MICU-1 expression via mRNA decay machinery. *car-1(0)* mutants have a higher MICU-1:MCU-1 ratio, causing increased $[Ca^{2+}]_{mt}$ uptake after axon injury and enhanced axon regrowth (Figure 7E). Axonal transport of mitochondria has been shown to boost regrowth in *C. elegans* and mammalian neurons [24–26]. Our observations suggest that more sustained $[Ca^{2+}]_{mt}$ uptake also promotes axon regrowth, for example potentially through increasing ATP production required for axon repair [61]. We speculate that the mild enhancement of $[Ca^{2+}]_{mt}$ uptake resulting from elevated MICU expression is insufficient to trigger deleterious consequences such as opening of the mitochondrial permeability transition pore that would lead to axonal degeneration. Precise modulation of $[Ca^{2+}]_{mt}$ uptake in injured neurons may provide new therapeutic routes toward effective axon repair.

STAR★METHODS

Detailed methods are provided in the online version of this paper and include the following:

- KEY RESOURCES TABLE
- LEAD CONTACT AND MATERIALS AVAILABILITY
- EXPERIMENTAL MODEL AND SUBJECT DETAILS
- METHOD DETAILS
  - *C. elegans* genetics
  - Molecular cloning
  - Transgenic strain construction
  - CRISPR-mediated deletion alleles and GFP knock-in
  - Fluorescence microscopy and laser axotomy
  - Single-end enhanced crosslinking and immunoprecipitation (seCLIP)
  - Single molecule fluorescence *in situ* hybridization (smFISH)
- QUANTIFICATION AND STATISTICAL ANALYSIS
- DATA AND CODE AVAILABILITY

SUPPLEMENTAL INFORMATION

Supplemental Information can be found online at https://doi.org/10.1016/j.cub.2019.12.061.

ACKNOWLEDGMENTS

We thank Yao Yao and Xuefeng Meng for assistance in strain construction, Zhiping Wang for CasSCI vectors, and members of the Jin and Chisholm laboratories for discussions. We thank Michael Nonet for the mito-tagRFP marker. Some mutants were provided by the Japan National Bioresource Project or by the Caenorhabditis Genetics Center (funded by the NIH office of research infrastructure programs P40 OD010440). K.W.K. received Hallym University research funds (HRF-201809-014). This work was supported by

NIH grant R01 GM054657 to A.D.C., R01 NS093588 to A.D.C. and Y.J., and R01 HG004659 to G.W.Y.

AUTHOR CONTRIBUTIONS

N.H.T., Y.J., and A.D.C. conceived the project. N.H.T. performed all experiments unless otherwise specified. K.W.K. performed smFISH experiments in Figures 1A and S1. S.X. generated *micu-1(0)* mutants. S.B., B.A.Y., and G.W.Y. contributed to seCLIP analyses. N.H.T., Y.J., and A.D.C. analyzed data and wrote the manuscript, with input from all authors.

DECLARATION OF INTERESTS

G.W.Y. is a co-founder and member of the Board of Directors, on the SAB, an equity holder, and a paid consultant for Locana and Eclipse BioInnovations. G.W.Y. is a visiting professor at the National University of Singapore, with the terms of this arrangement reviewed and approved by the University of California, San Diego in accordance with its conflict of interest policies. The other authors declare no competing financial interests.

Received: September 11, 2019
Revised: November 26, 2019
Accepted: December 19, 2019
Published: January 23, 2020

REFERENCES

1. Decker, C.J., and Parker, R. (2012). P-bodies and stress granules: possible roles in the control of translation and mRNA degradation. Cold Spring Harb. Perspect. Biol. *4*, a012286.
2. Grudzien-Nogalska, E., and Kiledjian, M. (2017). New insights into decapping enzymes and selective mRNA decay. Wiley Interdiscip. Rev. RNA *8*.
3. Barbee, S.A., Estes, P.S., Cziko, A.M., Hillebrand, J., Luedeman, R.A., Coller, J.M., Johnson, N., Howlett, I.C., Geng, C., Ueda, R., et al. (2006). Staufen- and FMRP-containing neuronal RNPs are structurally and functionally related to somatic P bodies. Neuron *52*, 997–1009.
4. Cougot, N., Bhattacharyya, S.N., Tapia-Arancibia, L., Bordonné, R., Filipowicz, W., Bertrand, E., and Rage, F. (2008). Dendrites of mammalian neurons contain specialized P-body-like structures that respond to neuronal activation. J. Neurosci. *28*, 13793–13804.
5. Hillebrand, J., Pan, K., Kokaram, A., Barbee, S., Parker, R., and Ramaswami, M. (2010). The Me31B DEAD-Box Helicase Localizes to Postsynaptic Foci and Regulates Expression of a CaMKII Reporter mRNA in Dendrites of Drosophila Olfactory Projection Neurons. Front. Neural Circuits *4*, 121.
6. Antonacci, S., Forand, D., Wolf, M., Tyus, C., Barney, J., Kellogg, L., et al. (2015). Conserved RNA-binding proteins required for dendrite morphogenesis in *Caenorhabditis elegans* sensory neurons. G3 (Bethesda) *5*, 639–653.
7. Audhya, A., Hyndman, F., McLeod, I.X., Maddox, A.S., Yates, J.R., 3rd, Desai, A., et al. (2005). A complex containing the Sm protein CAR-1 and the RNA helicase CGH-1 is required for embryonic cytokinesis in *Caenorhabditis elegans*. J. Cell Biol. *171*, 267–279.
8. Boag, P.R., Nakamura, A., and Blackwell, T.K. (2005). A conserved RNA-protein complex component involved in physiological germline apoptosis regulation in *C. elegans*. Development *132*, 4975–4986.
9. Lall, S., Piano, F., and Davis, R.E. (2005). *Caenorhabditis elegans* decapping proteins: localization and functional analysis of Dcp1, Dcp2, and DcpS during embryogenesis. Mol. Biol. Cell *16*, 5880–5890.
10. Squirrell, J.M., Eggers, Z.T., Luedke, N., Saari, B., Grimson, A., Lyons, G.E., et al. (2006). CAR-1, a protein that localizes with the mRNA decapping component DCAP-1, is required for cytokinesis and ER organization in *Caenorhabditis elegans* embryos. Mol. Biol. Cell *17*, 336–344.
11. Marnef, A., Sommerville, J., and Ladomery, M.R. (2009). RAP55: insights into an evolutionarily conserved protein family. Int. J. Biochem. Cell Biol. *41*, 977–981.
12. Sun, Y., Yang, P., Zhang, Y., Bao, X., Li, J., Hou, W., et al. (2011). A genome-wide RNAi screen identifies genes regulating the formation of P bodies in *C. elegans* and their functions in NMD and RNAi. Protein Cell *2*, 918–939.
13. Hammell, C.M., Lubin, I., Boag, P.R., Blackwell, T.K., and Ambros, V. (2009). nhl-2 Modulates microRNA activity in *Caenorhabditis elegans*. Cell *136*, 926–938.
14. Brandmann, T., Fakim, H., Padamsi, Z., Youn, J.Y., Gingras, A.C., Fabian, M.R., and Jinek, M. (2018). Molecular architecture of LSM14 interactions involved in the assembly of mRNA silencing complexes. EMBO J. *37*, e97869.
15. Teixeira, D., and Parker, R. (2007). Analysis of P-body assembly in *Saccharomyces cerevisiae*. Mol. Biol. Cell *18*, 2274–2287.
16. Wu, Z., Ghosh-Roy, A., Yanik, M.F., Zhang, J.Z., Jin, Y., and Chisholm, A.D. (2007). *Caenorhabditis elegans* neuronal regeneration is influenced by life stage, ephrin signaling, and synaptic branching. Proc. Natl. Acad. Sci. USA *104*, 15132–15137.
17. Bradke, F., Fawcett, J.W., and Spira, M.E. (2012). Assembly of a new growth cone after axotomy: the precursor to axon regeneration. Nat. Rev. Neurosci. *13*, 183–193.
18. Chen, L., Wang, Z., Ghosh-Roy, A., Hubert, T., Yan, D., O'Rourke, S., et al. (2011). Axon regeneration pathways identified by systematic genetic screening in *C. elegans*. Neuron *71*, 1043–1057.
19. Tedeschi, A., Dupraz, S., Curcio, M., Laskowski, C.J., Schaffran, B., Flynn, K.C., Santos, T.E., Stern, S., Hilton, B.J., Larson, M.J.E., et al. (2019). ADF/Cofilin-Mediated Actin Turnover Promotes Axon Regeneration in the Adult CNS. Neuron *103*, 1073–1085.e6.
20. Zeidan, Q., He, F., Zhang, F., Zhang, H., Jacobson, A., and Hinnebusch, A.G. (2018). Conserved mRNA-granule component Scd6 targets Dhh1 to repress translation initiation and activates Dcp2-mediated mRNA decay in vivo. PLoS Genet. *14*, e1007806.
21. Van Nostrand, E.L., Nguyen, T.B., Gelboin-Burkhart, C., Wang, R., Blue, S.M., Pratt, G.A., Louie, A.L., and Yeo, G.W. (2017). Robust, Cost-Effective Profiling of RNA Binding Protein Targets with Single-end Enhanced Crosslinking and Immunoprecipitation (seCLIP). Methods Mol. Biol. *1648*, 177–200.
22. Van Nostrand, E.L., Pratt, G.A., Shishkin, A.A., Gelboin-Burkhart, C., Fang, M.Y., Sundararaman, B., Blue, S.M., Nguyen, T.B., Surka, C., Elkins, K., et al. (2016). Robust transcriptome-wide discovery of RNA-binding protein binding sites with enhanced CLIP (eCLIP). Nat. Methods *13*, 508–514.
23. Kim, K.W., Tang, N.H., Piggott, C.A., Andrusiak, M.G., Park, S., Zhu, M., et al. (2018). Expanded genetic screening in *Caenorhabditis elegans* identifies new regulators and an inhibitory role for NAD+ in axon regeneration. eLife *7*, e39756.
24. Cartoni, R., Norsworthy, M.W., Bei, F., Wang, C., Li, S., Zhang, Y., Gabel, C.V., Schwarz, T.L., and He, Z. (2016). The Mammalian-Specific Protein Armcx1 Regulates Mitochondrial Transport during Axon Regeneration. Neuron *92*, 1294–1307.
25. Han, S.M., Baig, H.S., and Hammarlund, M. (2016). Mitochondria Localize to Injured Axons to Support Regeneration. Neuron *92*, 1308–1323.
26. Zhou, B., Yu, P., Lin, M.Y., Sun, T., Chen, Y., and Sheng, Z.H. (2016). Facilitation of axon regeneration by enhancing mitochondrial transport and rescuing energy deficits. J. Cell Biol. *214*, 103–119.
27. Baughman, J.M., Perocchi, F., Girgis, H.S., Plovanich, M., Belcher-Timme, C.A., Sancak, Y., Bao, X.R., Strittmatter, L., Goldberger, O., Bogorad, R.L., et al. (2011). Integrative genomics identifies MCU as an essential component of the mitochondrial calcium uniporter. Nature *476*, 341–345.
28. De Stefani, D., Raffaello, A., Teardo, E., Szabò, I., and Rizzuto, R. (2011). A forty-kilodalton protein of the inner membrane is the mitochondrial calcium uniporter. Nature *476*, 336–340.

29. Kirichok, Y., Krapivinsky, G., and Clapham, D.E. (2004). The mitochondrial calcium uniporter is a highly selective ion channel. Nature *427*, 360–364.
30. Mallilankaraman, K., Doonan, P., Cárdenas, C., Chandramoorthy, H.C., Müller, M., Miller, R., Hoffman, N.E., Gandhirajan, R.K., Molgó, J., Birnbaum, M.J., et al. (2012). MICU1 is an essential gatekeeper for MCU-mediated mitochondrial Ca(2+) uptake that regulates cell survival. Cell *151*, 630–644.
31. Perocchi, F., Gohil, V.M., Girgis, H.S., Bao, X.R., McCombs, J.E., Palmer, A.E., and Mootha, V.K. (2010). MICU1 encodes a mitochondrial EF hand protein required for Ca(2+) uptake. Nature *467*, 291–296.
32. Ghosh-Roy, A., Wu, Z., Goncharov, A., Jin, Y., and Chisholm, A.D. (2010). Calcium and cyclic AMP promote axonal regeneration in *Caenorhabditis elegans* and require DLK-1 kinase. J. Neurosci. *30*, 3175–3183.
33. Csordás, G., Golenár, T., Seifert, E.L., Kamer, K.J., Sancak, Y., Perocchi, F., Moffat, C., Weaver, D., de la Fuente Perez, S., Bogorad, R., et al. (2013). MICU1 controls both the threshold and cooperative activation of the mitochondrial Ca^{2+} uniporter. Cell Metab. *17*, 976–987.
34. Liu, J.C., Liu, J., Holmström, K.M., Menazza, S., Parks, R.J., Fergusson, M.M., Yu, Z.X., Springer, D.A., Halsey, C., Liu, C., et al. (2016). MICU1 Serves as a Molecular Gatekeeper to Prevent In Vivo Mitochondrial Calcium Overload. Cell Rep. *16*, 1561–1573.
35. Nishimura, T., Padamsi, Z., Fakim, H., Milette, S., Dunham, W.H., Gingras, A.C., and Fabian, M.R. (2015). The eIF4E-Binding Protein 4E-T Is a Component of the mRNA Decay Machinery that Bridges the 5′ and 3′ Termini of Target mRNAs. Cell Rep. *11*, 1425–1436.
36. Tanaka, K.J., Ogawa, K., Takagi, M., Imamoto, N., Matsumoto, K., and Tsujimoto, M. (2006). RAP55, a cytoplasmic mRNP component, represses translation in Xenopus oocytes. J. Biol. Chem. *281*, 40096–40106.
37. Nissan, T., Rajyaguru, P., She, M., Song, H., and Parker, R. (2010). Decapping activators in *Saccharomyces cerevisiae* act by multiple mechanisms. Mol. Cell *39*, 773–783.
38. Kwon, S., Zhang, Y., and Matthias, P. (2007). The deacetylase HDAC6 is a novel critical component of stress granules involved in the stress response. Genes Dev. *21*, 3381–3394.
39. Buchan, J.R., Muhlrad, D., and Parker, R. (2008). P bodies promote stress granule assembly in *Saccharomyces cerevisiae*. J. Cell Biol. *183*, 441–455.
40. Giorgi, C., Marchi, S., and Pinton, P. (2018). The machineries, regulation and cellular functions of mitochondrial calcium. Nat. Rev. Mol. Cell Biol. *19*, 713–730.
41. Kamer, K.J., and Mootha, V.K. (2015). The molecular era of the mitochondrial calcium uniporter. Nat. Rev. Mol. Cell Biol. *16*, 545–553.
42. Logan, C.V., Szabadkai, G., Sharpe, J.A., Parry, D.A., Torelli, S., Childs, A.M., Kriek, M., Phadke, R., Johnson, C.A., Roberts, N.Y., et al.; UK10K Consortium (2014). Loss-of-function mutations in MICU1 cause a brain and muscle disorder linked to primary alterations in mitochondrial calcium signaling. Nat. Genet. *46*, 188–193.
43. Shamseldin, H.E., Alasmari, A., Salih, M.A., Samman, M.M., Mian, S.A., Alshidi, T., Ibrahim, N., Hashem, M., Faqeih, E., Al-Mohanna, F., and Alkuraya, F.S. (2017). A null mutation in MICU2 causes abnormal mitochondrial calcium homeostasis and a severe neurodevelopmental disorder. Brain *140*, 2806–2813.
44. Lewis-Smith, D., Kamer, K.J., Griffin, H., Childs, A.M., Pysden, K., Titov, D., Duff, J., Pyle, A., Taylor, R.W., Yu-Wai-Man, P., et al. (2016). Homozygous deletion in MICU1 presenting with fatigue and lethargy in childhood. Neurol. Genet. *2*, e59.
45. Qiu, J., Tan, Y.W., Hagenston, A.M., Martel, M.A., Kneisel, N., Skehel, P.A., Wyllie, D.J., Bading, H., and Hardingham, G.E. (2013). Mitochondrial calcium uniporter Mcu controls excitotoxicity and is transcriptionally repressed by neuroprotective nuclear calcium signals. Nat. Commun. *4*, 2034.
46. De Stefani, D., Rizzuto, R., and Pozzan, T. (2016). Enjoy the Trip: Calcium in Mitochondria Back and Forth. Annu. Rev. Biochem. *85*, 161–192.
47. Barrientos, G.C., Feng, W., Truong, K., Matthaei, K.I., Yang, T., Allen, P.D., Lopez, J.R., and Pessah, I.N. (2012). Gene dose influences cellular and calcium channel dysregulation in heterozygous and homozygous T4826I-RYR1 malignant hyperthermia-susceptible muscle. J. Biol. Chem. *287*, 2863–2876.
48. Villegas, R., Martinez, N.W., Lillo, J., Pihan, P., Hernandez, D., Twiss, J.L., and Court, F.A. (2014). Calcium release from intra-axonal endoplasmic reticulum leads to axon degeneration through mitochondrial dysfunction. J. Neurosci. *34*, 7179–7189.
49. Sarasija, S., Laboy, J.T., Ashkavand, Z., Bonner, J., Tang, Y., and Norman, K.R. (2018). Presenilin mutations deregulate mitochondrial Ca^{2+} homeostasis and metabolic activity causing neurodegeneration in *Caenorhabditis elegans*. eLife *7*, e33052.
50. Zhang, L., Wang, H., Zhou, X., Mao, L., Ding, K., and Hu, Z. (2019). Role of mitochondrial calcium uniporter-mediated Ca^{2+} and iron accumulation in traumatic brain injury. J. Cell. Mol. Med. *23*, 2995–3009.
51. Drago, I., and Davis, R.L. (2016). Inhibiting the Mitochondrial Calcium Uniporter during Development Impairs Memory in Adult Drosophila. Cell Rep. *16*, 2763–2776.
52. Márkus, N.M., Hasel, P., Qiu, J., Bell, K.F., Heron, S., Kind, P.C., Dando, O., Simpson, T.I., and Hardingham, G.E. (2016). Expression of mRNA Encoding Mcu and Other Mitochondrial Calcium Regulatory Genes Depends on Cell Type, Neuronal Subtype, and Ca2+ Signaling. PLoS ONE *11*, e0148164.
53. Cho, Y., Sloutsky, R., Naegle, K.M., and Cavalli, V. (2013). Injury-induced HDAC5 nuclear export is essential for axon regeneration. Cell *155*, 894–908.
54. Yan, D., Wu, Z., Chisholm, A.D., and Jin, Y. (2009). The DLK-1 kinase promotes mRNA stability and local translation in *C. elegans* synapses and axon regeneration. Cell *138*, 1005–1018.
55. Yan, D., and Jin, Y. (2012). Regulation of DLK-1 kinase activity by calcium-mediated dissociation from an inhibitory isoform. Neuron *76*, 534–548.
56. Vargas, M.E., Yamagishi, Y., Tessier-Lavigne, M., and Sagasti, A. (2015). Live Imaging of Calcium Dynamics during Axon Degeneration Reveals Two Functionally Distinct Phases of Calcium Influx. J. Neurosci. *35*, 15026–15038.
57. Gottschalk, B., Klec, C., Leitinger, G., Bernhart, E., Rost, R., Bischof, H., Madreiter-Sokolowski, C.T., Radulović, S., Eroglu, E., Sattler, W., et al. (2019). MICU1 controls cristae junction and spatially anchors mitochondrial Ca^{2+} uniporter complex. Nat. Commun. *10*, 3732.
58. Hoffman, N.E., Chandramoorthy, H.C., Shamugapriya, S., Zhang, X., Rajan, S., Mallilankaraman, K., Gandhirajan, R.K., Vagnozzi, R.J., Ferrer, L.M., Sreekrishnanilayam, K., et al. (2013). MICU1 motifs define mitochondrial calcium uniporter binding and activity. Cell Rep. *5*, 1576–1588.
59. Patron, M., Checchetto, V., Raffaello, A., Teardo, E., Vecellio Reane, D., Mantoan, M., Granatiero, V., Szabò, I., De Stefani, D., and Rizzuto, R. (2014). MICU1 and MICU2 finely tune the mitochondrial Ca2+ uniporter by exerting opposite effects on MCU activity. Mol. Cell *53*, 726–737.
60. Paillard, M., Csordás, G., Szanda, G., Golenár, T., Debattisti, V., Bartok, A., Wang, N., Moffat, C., Seifert, E.L., Spät, A., and Hajnóczky, G. (2017). Tissue-Specific Mitochondrial Decoding of Cytoplasmic Ca^{2+} Signals Is Controlled by the Stoichiometry of MICU1/2 and MCU. Cell Rep. *18*, 2291–2300.
61. Wu, D., Lee, S., Luo, J., Xia, H., Gushchina, S., Richardson, P.M., Yeh, J., Krügel, U., Franke, H., Zhang, Y., and Bo, X. (2018). Intraneural Injection of ATP Stimulates Regeneration of Primary Sensory Axons in the Spinal Cord. J. Neurosci. *38*, 1351–1365.
62. O'Hagan, R., Chalfie, M., and Goodman, M.B. (2005). The MEC-4 DEG/ENaC channel of *Caenorhabditis elegans* touch receptor neurons transduces mechanical signals. Nat. Neurosci. *8*, 43–50.
63. Zheng, Q., Ahlawat, S., Schaefer, A., Mahoney, T., Koushika, S.P., and Nonet, M.L. (2014). The vesicle protein SAM-4 regulates the processivity of synaptic vesicle transport. PLoS Genet. *10*, e1004644.
64. Akerboom, J., Chen, T.W., Wardill, T.J., Tian, L., Marvin, J.S., Mutlu, S., Calderón, N.C., Esposti, F., Borghuis, B.G., Sun, X.R., et al. (2012).

Optimization of a GCaMP calcium indicator for neural activity imaging. J. Neurosci. *32*, 13819–13840.

65. Noma, K., and Jin, Y. (2015). Optogenetic mutagenesis in *Caenorhabditis elegans*. Nat. Commun. *6*, 8868.
66. Paix, A., Folkmann, A., Rasoloson, D., and Seydoux, G. (2015). High Efficiency, Homology-Directed Genome Editing in *Caenorhabditis elegans* Using CRISPR-Cas9 Ribonucleoprotein Complexes. Genetics *201*, 47–54.
67. Friedland, A.E., Tzur, Y.B., Esvelt, K.M., Colaiácovo, M.P., Church, G.M., and Calarco, J.A. (2013). Heritable genome editing in *C. elegans* via a CRISPR-Cas9 system. Nat. Methods *10*, 741–743.
68. Dejima, K., Hori, S., Iwata, S., Suehiro, Y., Yoshina, S., Motohashi, T., et al. (2018). An Aneuploidy-Free and Structurally Defined Balancer Chromosome Toolkit for *Caenorhabditis elegans*. Cell Rep. *22*, 232–241.
69. Dickinson, D.J., Pani, A.M., Heppert, J.K., Higgins, C.D., and Goldstein, B. (2015). Streamlined Genome Engineering with a Self-Excising Drug Selection Cassette. Genetics *200*, 1035–1049.
70. Lovci, M.T., Ghanem, D., Marr, H., Arnold, J., Gee, S., Parra, M., Liang, T.Y., Stark, T.J., Gehman, L.T., Hoon, S., et al. (2013). Rbfox proteins regulate alternative mRNA splicing through evolutionarily conserved RNA bridges. Nat. Struct. Mol. Biol. *20*, 1434–1442.
71. Kim, D., Langmead, B., and Salzberg, S.L. (2015). HISAT: a fast spliced aligner with low memory requirements. Nat. Methods *12*, 357–360.
72. Trapnell, C., Williams, B.A., Pertea, G., Mortazavi, A., Kwan, G., van Baren, M.J., Salzberg, S.L., Wold, B.J., and Pachter, L. (2010). Transcript assembly and quantification by RNA-Seq reveals unannotated transcripts and isoform switching during cell differentiation. Nat. Biotechnol. *28*, 511–515.
73. Trapnell, C., Hendrickson, D.G., Sauvageau, M., Goff, L., Rinn, J.L., and Pachter, L. (2013). Differential analysis of gene regulation at transcript resolution with RNA-seq. Nat. Biotechnol. *31*, 46–53.
74. Kim, K.W., Tang, N.H., Andrusiak, M.G., Wu, Z., Chisholm, A.D., and Jin, Y. (2018). A Neuronal piRNA Pathway Inhibits Axon Regeneration in *C. elegans*. Neuron *97*, 511–519.e6.

STAR★METHODS

KEY RESOURCES TABLE

REAGENT or RESOURCE	SOURCE	IDENTIFIER
Antibodies		
GFP Trap	ChromoTek	Cat#gtm-20; AB_2631359
Bacterial and Virus Strains		
E. coli: OP50-1	Caenorhabditis Genetics Center	RRID:WB-STRAIN:OP50-1
Chemicals, Peptides, and Recombinant Proteins		
Protein: Cas9-NLS purified protein	QB3 MacroLab, UC Berkeley	N/A
Stellaris RNA FISH Hybridization buffer	LGC BioSearch Technologies	Cat#SMF-HB1-10
Stellaris RNA FISH Wash Buffer A	LGC BioSearch Technologies	Cat#SMF-WA1-60
Stellaris RNA FISH Wash Buffer B	LGC BioSearch Technologies	Cat#SMF-WB1-20
ProLong Antifade Mountant with DAPI	Invitrogen	Cat#P36935
TRIzol Reagent	Invitrogen	Cat#15596026
DreamTaq DNA polymerases	Thermo Scientific	Cat#EP0705
Phusion High-Fidelity DNA polymerases	Thermo Scientific	Cat#F530L
Protease Inhibitor Cocktail Tablet	Roche	Cat#05892970001
Critical Commercial Assays		
SuperScript III First-Strand Synthesis System	Invitrogen	*Cat#18080051*
Gateway LR Clonase II Enzyme Mix	Thermo Scientific	Cat#11791-100
Gibson Assembly Master Mix	New England BioLabs	Cat#E2611S
Deposited Data		
Raw and Analyzed Data	This paper	GEO: GSE124714
Experimental Models: Organisms/Strains		
C. elegans: Strain wild type N2	Caenorhabditis Genetics Center	RRID:WB-STRAIN:N2_(ancestral)
C. elegans: Strain *Pmec-7-GFP(muIs32) II*	[18]	CZ10969
C. elegans: Strain *Pmec-4*-GFP*(zdIs5) I*	[18]	CZ10175
C. elegans: Strain *Pmec-17*-GFP*(uIs31) III*	[62]	CZ25265
C. elegans: Strain *zdIs5 I; [Pdcap-1*-DCAP-1::dsRed+*rol-6 (su1006)](bpIs37)*	This paper	CZ26592
C. elegans: Strain *Pmec-7-mRFP(jsIs973) III; Pcgh-1*-CGH-1:: GFP*(dhIs1000)*	This paper	CZ26244
C. elegans: Strain *Pcgh-1*-CGH-1::GFP*(dhIs1000); Pmec-4*-mKate2::CAR-1*(juEx7739)*	This paper	CZ25819
C. elegans: Strain *Pmec-4*-GFP::CAR-1*(juSi338) IV; [Pdcap-1*-DCAP-1::dsRed+*rol-6(su1006)](bpIs37)*	This paper	CZ25293
C. elegans: Strain *car-1(tm1753) I/hT2 [bli-4(e937) I let-?(q782) GFP(qIs48) I;III]; muIs32 II*	This paper	CZ11541
C. elegans: Strain *zdIs5 I; dcap-2(tm2470) IV*	This paper	CZ25658
C. elegans: Strain *zdIs5 I; cgh-1(ok492) III/hT2 [bli-4(e937) I let-?(q782) GFP(qIs48) I;III]*	This paper	CZ11540
C. elegans: Strain *zdIs5 I; dcap-1(ok2139) IV*	This paper	CZ11537
C. elegans: Strain *zdIs5 I; dcap-1(ok2139) dcap-2(tm2470) IV*	This paper	CZ27317
C. elegans: Strain *zdIs5 I; patr-1(tm2402) II/ mIn1 [mIs14 dpy-10(e128) II]*	This paper	CZ11759
C. elegans: Strain *car-1(tm1753) I/hT2 [bli-4(e937) I let-?(q782) GFP(qIs48) I;III]; uIs31 III*	This paper	CZ25319
C. elegans: Strain *muIs32 II; Pmec-4*-GFP::CAR-1*(juEx7280)*	This paper	CZ23991

(*Continued on next page*)

Continued

REAGENT or RESOURCE	SOURCE	IDENTIFIER
C. elegans: Strain *car-1(ju1505) I/hT2 [bli-4(e937) I let-?(q782) GFP(qIs48) I;III]; muIs32 II*	This paper	CZ25262
C. elegans: Strain *car-1(ju1506) I/hT2 [bli-4(e937) I let-?(q782) GFP(qIs48) I;III]; muIs32 II*	This paper	CZ25264
C. elegans: Strain *car-1(tm1753) I/hT2 [bli-4(e937) I let-?(q782) GFP(qIs48) I;III]; muIs32 II; loxP-Pcar-1*-GFP::*car-1g+3′UTR-loxP (juSi343) IV*	This paper	CZ25401
C. elegans: Strain *car-1(tm1753) I/hT2 [bli-4(e937) I let-?(q782) GFP(qIs48) I;III]; muIs32 II; Pmec-4*-GFP::CAR-1*(juSi338) IV*	This paper	CZ25112
C. elegans: Strain *car-1(tm1753) I/hT2 [bli-4(e937) I let-?(q782) GFP(qIs48) I;III]; Pmyo-3-car-1(juEx7913)*	This paper	CZ26723
C. elegans: Strain *Pmec-4*-GFP::CAR-1 *(juSi338) IV*	This paper	CZ24932
C. elegans: Strain *Pmec-4*-GFP::CAR-1(Sm) *(juSi346) IV*	This paper	CZ25350
C. elegans: Strain *Pmec-4*-GFP::CAR-1(ΔSm) *(juSi345) IV*	This paper	CZ25325
C. elegans: Strain *Pmec-4*-GFP::CAR-1(Sm+FDF) *(juSi349) IV*	This paper	CZ25432
C. elegans: Strain *Pmec-4*-GFP::CAR-1(RGG) *(juSi350) IV*	This paper	CZ25433
C. elegans: Strain *Pmec-4*-GFP::CAR-1(ΔFDF+RGG) *(juSi361) IV*	This paper	CZ25884
C. elegans: Strain *car-1(tm1753) I/hT2 [bli-4(e937) I let-?(q782) GFP(qIs48) I;III]; muIs32 II; Pmec-4-GFP::car-1(ΔSm) [juSi345] IV*	This paper	CZ25443
C. elegans: Strain *car-1(tm1753) I/hT2 [bli-4(e937) I let-?(q782) GFP(qIs48) I;III]; muIs32 II; Pmec-4-GFP::car-1(Sm) [juSi346] IV*	This paper	CZ25444
C. elegans: Strain *car-1(tm1753) I/hT2 [bli-4(e937) I let-?(q782) GFP(qIs48) I;III]; muIs32 II; Pmec-4-GFP::car-1(Sm+FDF) [juSi349] IV*	This paper	CZ25566
C. elegans: Strain *car-1(tm1753) I/hT2 [bli-4(e937) I let-?(q782) GFP(qIs48) I;III]; muIs32 II; Pmec-4-GFP::car-1(RGG) [juSi350] IV*	This paper	CZ25567
C. elegans: Strain *car-1(tm1753) I/hT2 [bli-4(e937) I let-?(q782) GFP(qIs48) I;III]; muIs32 II; Pmec-4-GFP::car-1(ΔFGF+RGG) [juSi361] IV*	This paper	CZ25938
C. elegans: Strain *zdIs5 I; Prgef-1-GFP::car-1(juIs526)*	This paper	CZ25296
C. elegans: Strain *zdIs5 I; Prgef-1-GFP::car-1(ΔSm) (juIs549)*	This paper	CZ26634
C. elegans: Strain *dcap-2(tm2470) IV; Pmec-4*-GFP::CAR-1*(juSi338) IV*	This paper	CZ26429
C. elegans: Strain *Pmec-7*-tagRFP::mito*(jsIs1073)*	[63]	NM3573
C. elegans: Strain *car-1(tm1753) I/hT2 [bli-4(e937) I let-?(q782) GFP(qIs48) I;III]; Pmec-7*-tagRFP::mito*(jsIs1073)*	This paper	CZ27549
C. elegans: Strain *Pmec-7*-mRFP*(jsIs973) III; micu-1::GFP(ju1783) IV*	This paper	CZ27519
C. elegans: Strain *car-1(tm1753) I/hT2 [bli-4(e937) I let-?(q782) GFP(qIs48) I;III]; Pmec-7*-mRFP*(jsIs973) III; micu-1::GFP(ju1783) IV*	This paper	CZ27538
C. elegans: Strain *muIs32 II; mcu-1(ju1154) IV*	This paper	CZ20877
C. elegans: Strain *muIs32 II; micu-1(ju1155) IV/nT1 [qIs51 IV;V]*	This paper	CZ26661
C. elegans: Strain *muIs32 II; car-1(tm1753) I/hT2 [bli-4(e937) I let-?(q782) GFP(qIs48) I;III]; mcu-1(ju1154) IV*	This paper	CZ25925
C. elegans: Strain *muIs32; car-1(tm1753) I/hT2 [bli-4(e937) I let-?(q782) GFP(qIs48) I;III]; micu-1(ju1155) IV/tmC9 [In(glb-19 lgc-52 In(mec-3 unc-31)) IV]*	This paper	CZ27010
C. elegans: Strain *Pmec-7*-mRFP*(jsIs973) III; Pmec-4*-mito::GCaMP5*(juIs550)*	This paper	CZ26629
C. elegans: Strain *car-1(tm1753) I/hT2 [bli-4(e937) I let-?(q782) GFP(qIs48) I;III]; Pmec-7*-mRFP*(jsIs973) III; Pmec-4*-mito::GCaMP5*(juIs550)*	This paper	CZ26687
C. elegans: Strain *Pmec-7*-mRFP*(jsIs973) III; micu-1(ju1155) IV/nT1 [qIs51 IV;V]; Pmec-4*-mito::GCaMP5*(juIs550)*	This paper	CZ26737
C. elegans: Strain *Pmec-7*-mRFP*(jsIs973) III; mcu-1(ju1154) IV; Pmec-4*-mito::GCaMP5*(juIs550)*	This paper	CZ26857

(*Continued on next page*)

Continued

REAGENT or RESOURCE	SOURCE	IDENTIFIER
C. elegans: Strain *Pmec-7-mRFP(jsIs973) III; mcu-1(ju1154) micu-1(ju1156) IV/nT1 [qIs51 IV;V]; Pmec-4-mito::GCaMP5(juIs550)*	This paper	CZ26858
C. elegans: Strain *car-1(tm1753) I/hT2 [bli-4(e937) I let-?(q782) GFP(qIs48) I;III]; Pmec-7-*mRFP*(jsIs973) III; mcu-1(ju1154) IV; Pmec-4-*mito::GCaMP5*(juIs550)*	This paper	CZ27060
C. elegans: Strain *car-1(tm1753) I/hT2 [bli-4(e937) I let-?(q782) GFP(qIs48) I;III]; Pmec-7-*mRFP*(jsIs973) III; micu-1(ju1155) IV/tmC9 [In(glb-19 lgc-52 In(mec-3 unc-31)) IV]; Pmec-4-*mito::GCaMP5*(juIs550)*	This paper	CZ27061
C. elegans: Strain *Punc-17::*GFP*(vsIs48); [Pdcap-1-*DCAP-1::dsRed+*rol-6(su1006)](bpIs37)*	This paper	CZ26594
C. elegans: Strain *Punc-17::*mCherry*(nuIs321); Pcgh-1-*CGH-1::GFP*(dhIs1000)*	This paper	CZ26802
C. elegans: Strain *muIs32 II; [Pdcap-1-*DCAP-1::dsRed+*rol-6(su1006)](bpIs37)*	This paper	CZ26384
C. elegans: Strain *car-1(tm1753) I/hT2 [bli-4(e937) I let-?(q782) GFP(qIs48) I;III]; muIs32 II; [Pdcap-1-*DCAP-1::*dsRed+rol-6(su1006)](bpIs37)*	This paper	CZ26541
C. elegans: Strain *zdIs5 I; dcap-2(tm2470) IV; [Pdcap-1-*DCAP-1::*dsRed+rol-6(su1006)](bpIs37)*	This paper	CZ26419
C. elegans: Strain *zdIs5 I; patr-1(tm2402) II/ mIn1 [mIs14 dpy-10(e128) II]; [Pdcap-1-*DCAP-1::dsRed+*rol-6(su1006)](bpIs37)*	This paper	CZ26425
C. elegans: Strain *zdIs5 I; cgh-1(ok492) III/hT2 [bli-4(e937) I let-?(q782) GFP(qIs48) I;III]; [Pdcap-1-*DCAP-1::dsRed+*rol-6(su1006)](bpIs37)*	This paper	CZ26511
C. elegans: Strain *cgh-1(ok492) III/hT2 [bli-4(e937) I let-?(q782) GFP(qIs48) I;III]; Pmec-4-GFP::CAR-1(juSi338) IV*	This paper	CZ25879
C. elegans: Strain *patr-1(tm2402) II/ mIn1 [mIs14 dpy-10(e128) II]; Pmec-4-GFP::CAR-1(juSi338) IV*	This paper	CZ26426
C. elegans: Strain *dcap-2(tm2470) IV; Pmec-4-GFP::CAR-1(juSi338) IV*	This paper	CZ26429
C. elegans: Strain *dcap-1(ok2139) IV; Pmec-4-GFP::CAR-1(juSi338) IV*	This paper	CZ26532
C. elegans: Strain *dcap-2(tm2470) IV; Pmec-4-GFP::CAR-1(juSi338) IV; [Pdcap-1-*DCAP-1::dsRed+*rol-6(su1006)](bpIs37)*	This paper	CZ26632
C. elegans: Strain *micu-1::gfp(ju1783) IV*	This paper	CZ27508
C. elegans: Strain *Pmec-4-GFP::DCAP-1(juEx8024)*	This paper	CZ27378
C. elegans: Strain *zdIs5 I; mcu-1(ju1154) IV*	This paper	CZ21242
C. elegans: Strain *zdIs5 I; micu-1(ju1155) IV/nT1 [qIs51 IV;V]*	This paper	CZ27382
C. elegans: Strain *zdIs5 I; dcap-1(ok2139) mcu-1(ju1154) IV*	This paper	CZ27368
C. elegans: Strain *zdIs5 I; dcap-1(ok2139)/nT1 dcap-1(ok2139) micu-1(ju1155) IV*	This paper	CZ27381
C. elegans: Strain *muIs32 II; Pmec-7-*tagRFP::mito*(jsIs1073)*	This paper	CZ25635
C. elegans: Strain *car-1(tm1753) I/hT2 [bli-4(e937) I let-?(q782) GFP(qIs48) I;III]; muIs32 II; Pmec-7-*tagRFP::mito*(jsIs1073)*	This paper	CZ25651
C. elegans: Strain *muIs32 II; mcu-1(ju1154) IV; Pmec-7-*tagRFP::mito*(jsIs1073)*	This paper	CZ26537
C. elegans: Strain *muIs32 II; micu-1(ju1155) IV//tmC9 [In(glb-19 lgc-52 In(mec-3 unc-31)) Pmyo-2-*Venus*(tmIs1221)] IV; Pmec-7-*tagRFP::mito*(jsIs1073)*	This paper	CZ27030
C. elegans: Strain *zdIs5 I; Pmec-4-micu-1-gfp(juEx8048)*	This paper	CZ27739
C. elegans: Strain *zdIs5 I; Pmec-4-micu-1-gfp(juEx8050)*	This paper	CZ27756
C. elegans: Strain *Pmec-7-*mRFP*(jsIs973) III; Pmec-4-*mito::GCaMP5*(juIs550); Pmec-4-micu-1-gfp(juEx8048)*	This paper	CZ27764
C. elegans: Transgenic allele: N2 injected with 10 ng/μl of pCZGY2860 [*Pmec-4-GFP::car-1(genomic)::let-858_3′UTR*] and 5 ng/μl pCFJ90 [*Pmyo-2-mCherry*].	This paper	*juEx7280*

(*Continued on next page*)

Continued

REAGENT or RESOURCE	SOURCE	IDENTIFIER
C. elegans: Transgenic allele: N2 injected with 10 ng/μl pCZGY3372 [*Pmyo-3-car-1(cDNA)::let-858_3′UTR*] and 3 ng/μl pCFJ90[*Pmyo-2-mCherry*].	This paper	*juEx7913*
C. elegans: Transgenic allele: N2 injected with 10 ng/μl pCZGY3411 [*Pmec-4-GFP::dcap-1(cDNA)::let-858_3′UTR*] and 3 ng/μl pCFJ90 [*Pmyo-2-mCherry*].	This paper	*juEx8024*
C. elegans: Transgenic allele: N2 injected with 2 ng/μl pCZGY3416 [*Pmec-4-micu-1-gfp*] and 3 ng/μl pCFJ90[*Pmyo-2-mCherry*].	This paper	*juEx8048*
C. elegans: Transgenic allele: N2 injected with 10 ng/μl pCZGY3416 [*Pmec-4-micu-1-gfp*] and 3 ng/μl pCFJ90[*Pmyo-2-mCherry*].	This paper	*juEx8050*
C. elegans: Single-copy transgenic allele: N2 injected with 50ng/μL of pCZGY3366 [*Pcar-1(1062bp upstream)-GFP::car-1(genomic+768bp 3′UTR)*].	This paper	*juSi343*
C. elegans: Single-copy transgenic allele: N2 injected with 50ng/μL of pCZGY3362 [*Pmec-4-GFP::car-1(cDNA)::let-858_3′UTR*].	This paper	*juSi338*
C. elegans: Single-copy transgenic allele: N2 injected with 50ng/μL of pCZGY3367 [*Pmec-4-GFP::car-1(Sm)::let-858_3′UTR*].	This paper	*juSi346*
C. elegans: Single-copy transgenic allele: N2 injected with 50ng/μL of pCZGY3368 [*Pmec-4-GFP::car-1(ΔSm)::let-858_3′UTR*].	This paper	*juSi345*
C. elegans: Single-copy transgenic allele: N2 injected with 50ng/μL of pCZGY3369 [*Pmec-4-GFP::car-1(Sm+FDF)::let-858_3′UTR*].	This paper	*juSi349*
C. elegans: Single-copy transgenic allele: N2 injected with 50ng/μL of pCZGY3370 [*Pmec-4-GFP::car-1(RGG)::let-858_3′UTR*].	This paper	*juSi350*
C. elegans: Single-copy transgenic allele: N2 injected with 50ng/μL of pCZGY3371 [*Pmec-4-GFP::car-1(ΔFDF+RGG)::let-858_3′UTR*].	This paper	*juSi361*
C. elegans: Multi-copy transgenic allele: CZ20310 [*Pmex-5-his-72::miniSOG(juSi164) III unc-119(ed3) III*] injected with 10 ng/μl pCZGY3363 [*Prgef-1-GFP::car-1(genomic)::let-858_3′UTR*] and 3 ng/μl pCFJ90[*Pmyo-2-mCherry*].	This paper	*juIs526*
C. elegans: Multi-copy transgenic allele: CZ20310 [*Pmex-5-his-72::miniSOG(juSi164) III unc-119(ed3) III*] injected with 10 ng/μl pCZGY3364 [*Prgef-1-GFP::car-1(ΔSm)::let-858_3′UTR*] 3 ng/μl pCFJ90[*Pmyo-2-mCherry*].	This paper	*juIs549*
C. elegans: Multi-copy transgenic allele: N2 injected with 40 ng/μL of *Pmec-4-mito::GCaMP5* and treated with TMP/UV.	This paper	*juIs550*
C. elegans: GFP knock-in allele: N2 injected with 50 ng/μl of pCZGY3412, 50 ng/μl of pCZGY3413, 10 ng/μl of pCZGY3414, 3 ng/μl Pmyo-2-mCherry and 3 ng/μl of Pmyo-3-mCherry. Strains were treated with heat shock as described in Dickinson et al., 2015.	This paper	*ju1783*
Oligonucleotides		
Alt-R® CRISPR-Cas9 crRNA for *car-1*: to make *car-1(ju1505) and car-1(ju1506)* deletion: /AltR1/rCrA rArGrC rUrCrG rArCrA rUrCrC rGrUrU rArCrG rGrUrU rUrUrA rGrArG rCrUrA rUrGrC rU/AltR2/	This paper	N/A
Alt-R® CRISPR-Cas9 crRNA for *car-1*: to make *car-1(ju1505) and car-1(ju1506)* deletion: /AltR1/rCrU rArArU rCrUrU rGrCrU rUrCrC rGrArU rGrUrA rGrUrU rUrUrA rGrArG rCrUrA rUrGrC rU/AltR2/	This paper	N/A
Alt-R® CRISPR-Cas9 crRNA for *micu-1*: to make *micu-1(ju1155) and micu-1(ju1156)* deletion: /AltR1/rGrU rGrGrG rCrGrG rUrUrU rCrUrC rGrCrG rArCrG rGrUrU rUrUrA rGrArG rCrUrA rUrGrC rU/AltR2/	This paper	N/A
Alt-R® CRISPR-Cas9 crRNA for *micu-1*: to make *micu-1(ju1155) and micu-1(ju1156)* deletion: /AltR1/rArU rCrGrA rUrCrC rUrArA rCrGrA rArGrA rCrArG rGrUrU rUrUrA rGrArG rCrUrA rUrGrC rU/AltR2/	This paper	N/A

(*Continued on next page*)

Continued

REAGENT or RESOURCE	SOURCE	IDENTIFIER
Alt-R CRISPR-Cas9 tracrRNA	IDT	Cat#1072532
Recombinant DNA		
Plasmid: *Pmec-4-GFP::car-1(genomic)-let-858_3′UTR*	This paper	pCZGY2860
Plasmid: *FRT-Hygro-FRT-Pmec-4-GFP::car-1(cDNA)-let-858_3′UTR for CRISPR*	This paper	pCZGY3362
Plasmid: *Prgef-1-GFP::car-1(cDNA)-let-858_3′UTR*	This paper	pCZGY3363
Plasmid: *Prgef-1-GFP::car-1(ΔSm)-let-858_3′UTR*	This paper	pCZGY3364
Plasmid: *FRT-Hygro-FRT-loxP-car-1-loxP for CRISPR*	This paper	pCZGY3365
Plasmid: *FRT-Hygro-FRT-Pcar-1(1062bp upstream)-GFP::car-1(genomic+768bp 3′UTR) for CRISPR*	This paper	pCZGY3366
Plasmid: *FRT-Hygro-FRT-Pmec-4-GFP::car-1(Sm)-let-858_3′UTR for CRISPR*	This paper	pCZGY3367
Plasmid: *FRT-Hygro-FRT-Pmec-4-GFP::car-1(ΔSm)-let-858_3′UTR for CRISPR*	This paper	pCZGY3368
Plasmid: *FRT-Hygro-FRT-Pmec-4-GFP::car-1-(ΔRGG)-let-858_3′UTR for CRISPR*	This paper	pCZGY3369
Plasmid: *FRT-Hygro-FRT-Pmec-4-GFP::car-1(RGG)-let-858_3′UTR for CRISPR*	This paper	pCZGY3370
Plasmid: *FRT-Hygro-FRT-Pmec-4-GFP::car-1(ΔFDF+RGG)-let-858_3′UTR for CRISPR*	This paper	pCZGY3371
Plasmid: *Pmyo-3-car-1(cDNA)-unc-54_3′UTR*	This paper	pCZGY3372
Plasmid: *Pmec-4-GFP::dcap-1(cDNA)-let-858_3′UTR*	This paper	pCZGY3411
Plasmid: *Peft-3::Cas9+micu-1_C1_sgRNA*	This paper	pCZGY3412
Plasmid: *Peft-3::Cas9+micu-1_C2_sgRNA*	This paper	pCZGY3413
Plasmid: *GFP-SEC-3xFLAG_micu-1_C1_homology_arm*	This paper	pCZGY3414
Plasmid: *Pmec-4-micu-1-gfp*	This paper	pCZGY3416
Software and Algorithms		
ImageJ	NIH image	RRID:SCR_003070
GraphPad Prism 7	GraphPad Software, Inc.	RRID:SCR_002798
ZEN	Zeiss	https://www.zeiss.com/microscopy/us/downloads/zen.html

LEAD CONTACT AND MATERIALS AVAILABILITY

Further information and requests for reagents should be directed to and will be fulfilled by the Lead Contact, Andrew Chisholm (adchisholm@ucsd.edu). All unique/stable reagents generated in this study are available from the Lead Contact without restriction.

EXPERIMENTAL MODEL AND SUBJECT DETAILS

The nematode *Caenorhabditis elegans* was used as the experimental model for this study. All experiments were performed with hermaphrodite animals; males were used only for crosses. *C. elegans* strains were maintained at 20°C on nematode growth medium (NGM) agar plates seeded with *E. coli* OP50.

METHOD DETAILS

C. elegans genetics

car-1(0), *cgh-1(0)* and *patr-1(0)* mutants display maternal effect lethality, and *micu-1(0)* mutants display sterility. There mutants were kept as balanced strains. Homozygous *car-1(0)*, *cgh-1(0), patr-1(0)* and *micu-1(0)* mutants produced from heterozygous mothers were analyzed. *car-1(0)* and *micu-1(0)* mutants do not display overt behavioral or developmental phenotypes. We used the following transgenes: P*mec-7*-GFP*(muIs32)*, P*mec-4*-GFP*(zdIs5)*, P*mec-17*-GFP*(uIs31)* and P*mec-7*-mRFP*(jsIs973)* to visualize touch receptor neurons (TRNs), P*unc-17*-mCherry*(nuIs321)* and P*unc-17*-GFP*(vsIs48)* to visualize cholinergic motor neurons, and

P*mec-7*-mito-tagRFP*(jsIs1073)* to visualize mitochondria in TRNs. Different transgenes were used when possible to confirm that phenotypes are not transgene dependent. Transgenes were introduced to various mutants by standard genetic crossing.

Molecular cloning

To generate *car-1* rescue constructs, we cloned ~3kb of *car-1* genomic DNA into pCR8 vector. A full-length *car-1* cDNA was generated by RT-PCR from wild type N2 total RNA. Expression constructs for tagged or truncated CAR-1 were generated from cDNA by PCR and cloned into destination vectors containing P*mec-4* or P*myo-3* promoter using the Gateway system (Life Technologies). We expressed the Ca^{2+} sensor GCaMP5 [64] to the mitochondrial matrix (mtGCaMP) in TRNs using the *mec-4* TRN-specific promoter. We used Gibson assembly (New England Biolabs) to generate clones for single-copy transgenes.

Transgenic strain construction

For standard extrachromosomal transgenes, plasmid DNAs were used at 10 ng/μl, co-injection marker P*ttx-3*-RFP at 90 ng/μl or P*myo-2*-mCherry at 3-5 ng/μl. At least 2 independent transgenic lines were analyzed per construct. Single-copy transgenes were inserted into the transposon site *cxTi10882* on chromosome IV using CRISPR/Cas9. Three plasmids were injected into wild type hermaphrodites: a plasmid encoding Hyg^R+GFP-*car-1*-cDNA flanked by homology arms, a plasmid encoding Cas9+sgRNA, and a plasmid encoding co-injection marker. Animals were selected for genomic insertion based upon resistance to hygromycin (Hyg^R), the absence of co-injection markers and transgene was confirmed by PCR genotyping. We used optogenetic mutagenesis to generate chromosomal integration of pan-neuronal GFP-CAR-1 constructs [P*rgef-1*-GFP::CAR-1(FL)*(juIs527)* and P*rgef-1*-GFP::CAR-1(ΔSm)*(juIs549)*] [65]. Briefly, plasmids were injected into CZ20310 [P*mex-5*-HIS::miniSOG*(juSi164); unc-19(ed3)*] L4 hermaphrodites, and 6 h after injection, these animals were exposed to blue light for 30 min at 4 Hz. F1 progeny with co-injection marker were singled onto seeded plates. F2 progeny from F1 plates with > 75% transmission were singled, and those showing 100% transmission of the co-injection maker in the following generation were outcrossed with wild type males to confirm chromosomal integration. We also determined by quantitative PCR the copy number of the expression construct in *juIs526* and *juIs549* to be 52 and 78 copies respectively. P*mec-4*-mito-GCaMP5*(juIs550)* was integrated using UV-trimethylpsoralen and outcrossed 4 times before use.

CRISPR-mediated deletion alleles and GFP knock-in

We generated *car-1* deletions using two CRISPR RNA (crRNAs), 5′-CTAATCTTGCTTCCGATGTA-3′ and 5′-CAAGCTCGAC ATCCGTTACG-3′ (Integrated DNA Technologies) targeting the coding sequence in the first exon of *car-1*. The crRNAs were injected into wild type hermaphrodites with purified Cas9 (MacroLabs, University of California, Berkeley), *trans*-activating crRNA (tracrRNA) and *dpy-10* crRNA, as described [66]. Among 147 Dpy F1 worms, we identified two worms heterozygous for *car-1* deletions *ju1505* and *ju1506*. Like *car-1(tm1753)*, eggs laid by homozygous *car-1(ju1505)* and *car-1(ju1506)* worms failed to hatch, indicating all three alleles are null mutants. *car-1* alleles were balanced over *hT2* I; III [*bli-4(e937) I let-?(q782) GFP(qIs48)* I;III].

We generated *micu-1* deletion alleles as described [67]. We designed two subgenomic RNAs (sgRNAs): GTGG GCGGTTTCTCGCGACG and ATCGATCCTAACGAAGACAG. pU6::micu-1 sgRNAs were generated by primer annealing and injected into wild type or *mcu-1(ju1154)* worms as mixtures of 40 ng/μl of each pU6::*micu-1* sgRNA, 100 ng/μl of P*eft-3*-Cas9-SV40 NLS::tbb-2_3′UTR, and 20 ng/μl of P*col-19*-GFP as coinjection marker. We obtained worms heterozygous for *micu-1(ju1155)* in N2 background and *micu-1(ju1156)* in *mcu-1(ju1154)* background. *micu-1* alleles were balanced over *nT1 IV; V [qIs51]* or *tmC9 [In(glb-19 lgc-52 In(mec-3 unc-31)) IV* [68].

We inserted GFP at the C terminus of *micu-1* using the self-excising drug selection cassette [69]. We designed two subgenomic RNAs (sgRNAs): CTAATAAAATGGAAGAGGAC and ATGGCCACTGTAAATACTTG. We injected 50 ng/μl of each *micu-1* sgRNA, 10 ng/μl of homology arm repair template, 3 ng/μl Pmyo-2-mCherry and 3 ng/μl of Pmyo-3-mCherry into wild type worms. New alleles are in Table S2.

Fluorescence microscopy and laser axotomy

Fluorescence images were collected using Zeiss LSM510, LSM710, or LSM800 confocal microscopes, unless specified. Laser axotomy was performed as described [16, 18]. Images shown were projected as z stack. For live imaging of GCaMP fluorescence, we collected images every 240 ms using the spinning-disk confocal. Femtosecond laser power was 140 to180 mW with a shutter time of 1.2–1.5 ms. The mitochondrion closest to the axotomy site in the proximal axon was set as the region of interest (ROI). We outlined the mitochondrion and measured its integrated density using ImageJ and subtracted the integrated density from background using an identical outline within the axon to obtain net fluorescence (F). Baseline fluorescence (F0) was obtained from the ROI one frame before axotomy. The change in fluorescence ΔF was expressed as the ratio of change with respect to the baseline.

Single-end enhanced crosslinking and immunoprecipitation (seCLIP)

We performed single-end enhanced crosslinking and immunoprecipitation (seCLIP) as previously described [21] with a few modifications. Worms expressing pan-neuronal GFP::CAR-1 [P*rgef-1*-GFP::CAR-1*(juIs527)*] or pan-neuronal GFP::CAR-1(ΔSm) [P*rgef-1*-GFP::CAR-1(ΔSm)*(juIs549)*] were UV-crosslinked at 3 kJ/m^2 then resuspended in lysis buffer [50 mM Tris-HCl pH7.4, 100 mM NaCl, 1% NP-40, 0.1% SDS, 0.5% sodium deoxycholate, supplemented with one tablet of protease inhibitor cocktail tablet (Roche) in 20 ml]. Subsequent steps were performed as described [21]. Immunoprecipitation was performed using GFP-Trap (ChromoTek). Washes were performed using lysis buffer instead of high salt wash buffer. The quality of sequencing reads from fastq

files was evaluated by FastQC (http://www.bioinformatics.babraham.ac.uk/projects/fastqc). Bioinformatic analysis of sequencing reads was performed as previously described [22].

43,905,923 and 64,702,729 reads were obtained from GFP::CAR-1(FL) and GFP::CAR-1(ΔSm) sample respectively, of which 4,022,150 [CAR-1(FL)] and 5,470,606 [CAR-1(ΔSm)] reads uniquely mapped to *C. elegans* genome, after removing PCR duplicates and repeats. We identified 1190 genes with peaks > 2x enriched in CAR-1(ΔSm) over CAR-1(FL) (Table S1) using CLIPper peak calling [70]. Fold enrichment was calculated using the number of eCLIP reads overlapping CLIPper-identified peaks, after normalizing to total usable read counts in each sample. We also analyzed fastq files using HISAT2 [71], followed by transcript assembly using Cufflinks [72] and differential analysis using Cuffdiff (p value < 0.05) [73]. 29 genes were enriched in CLIPper and in Cufflinks-Cuffdiff analyses (Table S1). We inspected all genes enriched in CAR-1(ΔSm) and focused on *micu-1*, which showed 2x Peak enrichment in exon 7 at ChrIV:13299691-13299814.

Single molecule fluorescence *in situ* hybridization (smFISH)

Forty-eight 20-nt probes for *car-1* or *micu-1* mRNAs were designed and purchased from LGC BioSearch Technologies and conjugated to Cal Fluor 610. We performed smFISH using mixed stage animals according to a modified Stellaris protocol [74]. We used P*mec-7*-GFP*(muIs32)* or P*mec-4*-GFP*(zdIs5)* animals expressing GFP in TRNs as a reference for mRNA localization in PLM neurons. For imaging we used Leica DMi8 microscope, Andor spinning disk confocal (CSU-W1) and iXon ultra 888 EMCCD camera. All images shown are z stack projections.

QUANTIFICATION AND STATISTICAL ANALYSIS

Statistical tests were performed using GraphPad Prism. Two-way comparisons of categorical data were performed using Fisher's exact test. For multiple comparisons, we used one-way ANOVA with Bonferroni's post test. All data compared using unpaired Student's t test passed the D'Agostino & Pearson omnibus normality test. To compare regrowth between experiments with different control means, we normalized each experimental data point by dividing it by its control means. Sample sizes are indicated in Figures (dot plots) or in Figure legends.

DATA AND CODE AVAILABILITY

The raw and analyzed seCLIP datasets have been deposited at the Gene Expression Omnibus (accession number: GSE124714).